THESIS FOR THE DEGREE OF DOCTOR OF PHILOSOPHY

Modelling electrooxidation of glycerol and methanol on close-packed transition metal surfaces

MIKAEL VALTER

CHALMERS

Department of Physics
CHALMERS UNIVERSITY OF TECHNOLOGY
Göteborg, Sweden 2020

Modelling electrooxidation of glycerol and methanol on close-packed transition metal surfaces
MIKAEL VALTER
ISBN 978-91-7905-320-8

Doktorsavhandlingar vid Chalmers tekniska högskola
Ny serie nr. 4787
ISSN 0346-718X

Department of Physics
Chalmers University of Technology
SE-412 96 Göteborg
Sweden
Telephone: +46 (0)31-772 1000

Cover:
Products from partial glycerol electrooxidation on Au(111), Pt(111), and Cu(111). Image by Adam Arvidsson.

Chalmers digitaltryck
Göteborg, Sweden 2020

Modelling electrooxidation of glycerol and methanol on close-packed transition metal surfaces

MIKAEL VALTER
Department of Physics
Chalmers University of Technology

Abstract

Burning fossil fuels leads to excess CO_2 in the atmosphere, causing global warming, threatening civilisation and ecosystems worldwide. As a step in making the society fossil-independent, we need to replace oil, coal, and gas in the transportation sector with fuels originating from sustainable energy sources. Biodiesel is one such option, from which glycerol is a byproduct. With the help of electrooxidation, glycerol can be used as a feedstock to extract hydrogen gas, which may be used for upgrading biofuels or in proton exchange membrane (PEM) fuel cells. Methanol is a possible fuel in direct methanol fuel cells (DMFCs) and can, moreover, be used as a simple model for glycerol in some respects.

The primary focus of this thesis is to study the reaction thermodynamics of glycerol electrooxidation on Au(111) and other close-packed late transition metal surfaces. This provides routes and products that are thermodynamically favourable, information on steps that are difficult to overcome, and at what theoretical limiting potential the reaction becomes spontaneous. Using scaling relations for adsorption energies, these results can be generalised to alloys and other possible electrode materials. We use density functional theory to model the system, and to some extent experimental verification by cyclic voltammetry. Long range dispersion (van der Waals), which have been neglected in computations until recently, is investigated by assessing density van der Waals functionals. This is of particular importance for an inert metal such as gold. Another aspect that has commonly been ignored is solvent effects, which we study for the model system of methanol electrooxidation on Au(111). This includes an implicit model – a continuous dielectric – and an explicit model of water molecules.

Keywords: DFT, electrochemistry, biodiesel, glycerol, methanol, gold, Au(111), transition metals, van der Waals, implicit solvation, scaling relations

List of Publications

This thesis is based on the following appended papers:

Paper I:

Geometry and Electronic Properties of Glycerol Adsorbed on Bare and Transition-Metal Surface-Alloyed Au(111): A Density Functional Theory Study
Jonas Baltrusaitis, Mikael Valter, and Anders Hellman
J. Chem. Phys. C **120** (2016), 1749–1757

Paper II:

Electrooxidation of Glycerol on Gold in Acidic Medium: A Combined Experimental and DFT Study
Mikael Valter, Michael Busch, Björn Wickman, Henrik Grönbeck, Jonas Baltrusaitis, and Anders Hellman
J. Phys. Chem. C, **122** (2018), 10489-10494

Paper III:

Partial Electrooxidation of Glycerol on Close-Packed Transition Metal Surfaces: Insights from First-Principles Calculations
Mikael Valter, Egon Campos dos Santos, Lars G. M. Pettersson, and Anders Hellman
Submitted

Paper IV:

Selectivity of the First Two Glycerol Dehydrogenation Steps Determined Using Scaling Relationships
Mikael Valter, Egon Campos dos Santos, Lars G. M. Pettersson, and Anders Hellman
In manuscript

Paper V:

Solvent Effects for Methanol Electrooxidation on Gold
Mikael Valter and Anders Hellman
In manuscript

My contributions to the publications

Paper I
I performed the benchmarking calculations on gold properties (Table 1) and co-authored the manuscript.

Paper II
I performed all the calculations and experiments and was the main responsible for writing the manuscript.

Paper III
I performed all calculations and was the main responsible for writing the manuscript.

Paper IV
I performed most calculations and co-authored the manuscript.

Paper V
I performed all calculations and experiments and co-authored the manuscript.

Contents

Chapter 1

Introduction

While what we now call catalysis has been used throughout history, e.g. in fermentation of sugar to alcohol, there has not been any recorded attempts to characterise and explain the phenomenon until around 1800.[1] In 1794, the Scottish chemist Elizabeth Fulhame described how water facilitates oxidation and reduction reactions. She explained that the reactions are dependent on the presence of water, that water was directly involved in the chemical process and that the amount of water remained the same at the start and the end of the reaction.[2] This property of the water, that it enables or facilitates a reaction without being consumed itself, makes it a *catalyst*. This term is derived from *catalysis* (from Greek: $\kappa\alpha\tau\alpha$, 'down', and $\lambda\upsilon\epsilon\iota\nu$, 'loosen'),[3] coined by the Swedish chemist Jöns Jacob Berzelius 40 years later.[4] Catalysis has since then grown to an important chemical field. An important point in history was the invention of the Haber–Bosch process – synthesis of ammonia (NH_3) from hydrogen and nitrogen with an iron catalyst – in the beginning of the 20th century.[5–7] The new, effective method of producing artificial fertiliser revolutionalised global agriculture, allowing for a population growth from 1.6 billion in 1900 to 7.8 billion today. Catalysis has proven useful for a number of other processes in the chemical industry; crude oil is catalytically cracked to shorter carbon chains, e.g. gasoline, with the help of zeolites.[8]; selective oxidation of ethylene to ethylene epoxide is carried out directly using a silver catalyst, instead of an earlier multi-step process requiring chlorine gas.[9] As concerns for health and environment have increased towards the later part of the 20th century, catalytic processes for exhaust treatment have been developed. Examples of these are NO_x reduction[10] and CO oxidation[11, 12] in combustion engines.

Another modern application is energy conversion and storage, such as batteries and fuel cells, which belong to a certain class of catalysis involving electrochemistry. Electrochemistry is the relationship between chemical and electrical energy, which can be understood by describing the electrochemical cell (Figure 1.1).[13] This consists typically of two solid electrodes, the anode and the cathode, connected to each other via a power source or load and an electrolyte. The electrolyte is normally a liquid and its purpose is to conduct ions between the electrodes. The electrons, on the other hand, pass through the wire from the anode to the cathode giving rise to or being driven by a potential. The reaction, including charge transfer, takes place at the surface of the electrode. As long as the electrode is not consumed, it is a catalyst by definition. To stress the catalytic nature of the process, the term *electrocatalysis* was used by Kobozev and Monblanova in the 1930s when studying the kinetics of the hydrogen evolution reaction (HER)[14][1], where protons and electrons combine to form hydrogen gas,

$$2\,H^+ + 2\,e^- \longrightarrow H_2, \tag{1.1}$$

[1] To the best of my knowledge, the term is coined in this paper.

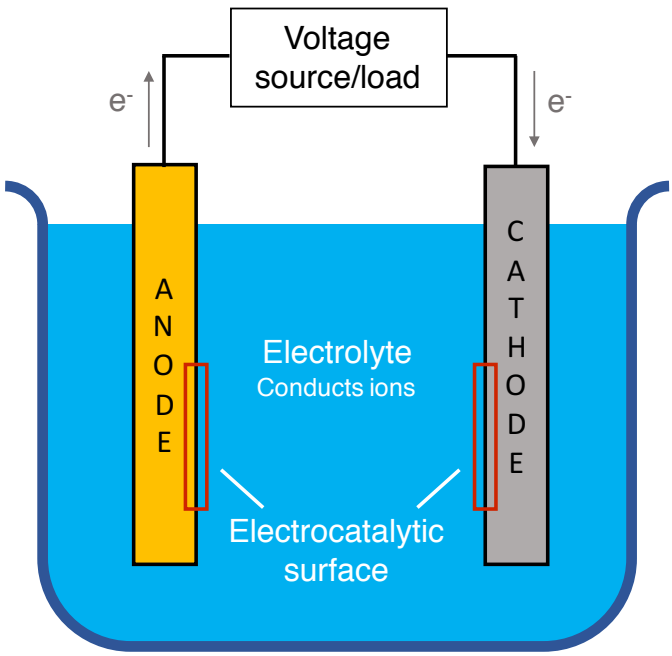

Figure 1.1: Sketch of a simple electrochemical cell. The electrons travel from the anode to the cathode via a voltage source (electrolytic cell) or a load (galvanic cell). Charged ions are moving through the electrolyte to retain charge neutrality. The reactions occur on the electrode surfaces, which acts as catalysts in the sense that they can be more or less effective at facilitating the electrochemical reactions.

on different metals. It should be pointed out that electrocatalysis is not really a subcategory of electrochemistry; there is no zero-activity electrode, and thus no non-catalysed reaction. Electrocatalysis refers to relative catalytic properties of possible electrode materials.[13]

1.1 Motivation

Today, fuels are generally produces from fossil sources.[15, 16] The use of fossil fuels leads to emission of CO_2 in the atmosphere, which have been shown to cause global warming.[17, 18] The climate change, being rapid in a geological perspective, is devastating to slowly-adapting ecosystems[19] and to human civilisation.[20, 21] In order to decrease CO_2 emissions, we need to replace oil, coal, and gas with sustainable sources of energy. Alternative fuel solutions include, as mentioned above, fuel cells and batteries (coupled with non-fossil primary energy sources), to which biodiesel can be added. Biodiesel is produced via esterification of fatty acids from vegetable oils and animal fats. Millions of metric tonnes of glycerol is produced annually as a byproduct in this process. While there are uses for glycerol, e.g. as a humectant (moist keeper) in cosmetics and pharmaceuticals[22], the supply vastly exceed the demand.[23] As an alternative to dispose of it as waste, which can lead to production of toxic products, it can be converted to more valuable products through various processes, such as reforming, hydrogenolysis, esterification, pyrolysis, carboxylation, oligomerisation, and polymerisation.[23, 24] Compared to most of these methods, electrooxidation has the advantage of being run at normal pressure and temperature and the potential of high yield and selectivity. Electrooxidation products include formic acid (FA), which is used in agriculture and in the leather industry,[25] tartronic acid (TA), which can be used as an oxygen scavenger[26], dihydroxyacetone (DHA), which is used as starting material in D, L-serin synthesis and as tanning agent in cosmetics, [27] glyceraldehyde (GLYD), which can be found in skin care products [27], glyceric acid (GLYC), which is used in medical applications, [26] and hydroxypyruvic acid (HYDP). Furthermore, glycerol electrooxidation will produce H_2, which has a wide range of applications, such as fuel cells, upgrading biofuels via hydrogenation of unsaturated fatty methyl esters,[28] or steel production, which is being tested in Sweden.[29] If only H_2 is of interest, glycerol can be fully oxidized to CO_2 and H_2 at a standard potential of 0.003 V vs. RHE, which can be compared to water splitting that ideally requires 1.23 V vs. RHE.[30]

Methanol electrooxidation can be seen as a prototypical reaction, used for benchmarking and as a model system for glycerol. In addition, methanol can be used for energy storage by using direct methanol fuel cells (DMFC) to generate electricity, which has grown in interest recently.[31]

1.2 Scope

The main aim of this thesis is to use electronic structure calculations to study surface reaction mechanisms for glycerol electrooxidation, in order to search for optimal electrocatalysts. We use Au(111) and other close-packed late transition metal surfaces as models, from which we generalise with scaling relations relating selectivity to carbon and

oxygen bonding, which allows for finding alloys and other surfaces. The calculations, performed with density functional theory, is used to determine binding and vibration energies, which in turn is used to calculate reaction intermediates and paths, as well as theoretical limiting potentials. The work is restricted to thermodynamics, excluding calculations on kinetics and transport processes. Along the work, we have studied several methodological issues. We have, for example, investigated the potential-dependent surface conditions for Au(111), long range dispersion for methanol adsorption and the impact of implicit and explicit solvation models and on methanol electrooxidation, as well as carried out experimental verification by cyclic voltammetry.

The outline of this thesis is that we start by discussing the theory of electrocatalysis in Chapter 2, leading up to understanding how to construct a suitable computational model. Chapter 3 outlines density functional theory, an application of quantum mechanics, to calculate energies of atomic systems. In order to use these energies to calculate measurable properties such as vibration frequencies and reaction free energies, we discuss e.g. vibrational analysis and semi-classical thermodynamics in Chapter 4. A summary of the important results of the papers, followed by discussion and outlook, is given in Chapter 5.

Chapter 2

Electrocatalysis

> “
> Let us now analyse the situation for natural forms of diffusion, occlusion and catalysis, where the first step is always the ‘natural’ adsorption of the component, and their ‘forced’ form, e.g. electroocclusion, electrodiffusion or electrocatalysis, where H atoms are forcibly formed in the final state at the membrane by the electrical current.
>
> – Nikolai Ivanovich Kobozev and Valentina Viktorovna Monblanova [14]

As already mentionned, electrocatalysis has emerged as a cross-disciplinary field between electrochemistry and catalysis. To introduce this field, we discuss catalysis and electrochemistry separately.

2.1 Catalysis

Let us assume that we have an non-catalysed reaction in gas phase with reactants A and B and the product P,[9]

$$\mathrm{A} + \mathrm{B} \longrightarrow \mathrm{P}. \tag{2.1}$$

As the reaction can occur only during the short time scales when the reactants are in contact, we approximate the reaction with one single step. This also means that the rate r will be proportional to the number of collisions and thus to the partial pressures p_i,

$$r_+ = p_\mathrm{A} p_\mathrm{B} k_+ \tag{2.2}$$

where k_+ is the rate constant, and the plus denotes the forward reaction (from left to right in Equation 2.1). The reactants need to overcome an energy barrier, corresponding to breaking and forming chemical bonds. The energy required to overcome the barrier is called *activation energy*, E_A, and must in this case come from the kinetic energy of the molecules. At any given temperature, T, there is a distribution of kinetic energy among the molecules such that a portion of them can overcome E_A. As the average kinetic energy increases linearly with temperature, it can be argued that the rate constant should be

$$k_+ = A_+ e^{-\beta E_A}, \tag{2.3}$$

where A_+ the concentration-dependent preexponential factor and $\beta = \frac{1}{k_\mathrm{B} T}$, where k_B is the Boltzmann constant. Svante Arrhenius proposed this equation in 1889,[32, 33] and a similar result was derived from collision theory 27 years later.[34] The Arrhenius equation governs the *kinetics* of the reaction, i.e. the rate at which reaction barriers are overcome.

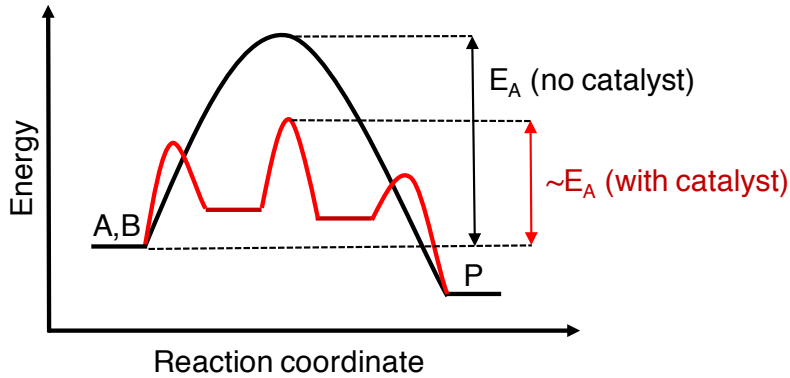

Figure 2.1: The effect of a catalyst in terms of energy barriers. The uncatalysed reaction (black) has fewer intermediate steps and can often be modelled as a single reaction associated with a single energy barrier. The catalyst introduces more well-defined intermediates with lower barriers (red), giving a lower effective barrier for the reaction. The figure is adapted from Wikimedia Commons.[35]

This is in contrast with the macroscopic reaction rate, the *activity* (not to be confused with thermodynamic activity), which might be influenced by e.g. transport limitations.[9]

In the presence of a catalyst, reactants will form bonds to it via its *active site*, while loosening their own intramolecular bonds. In addition to an easier bond breaking, the catalyst allows the formation of intermediates. This means that the catalysed reaction can have several well-defined elementary steps, each associated with a smaller reaction barrier compared to the large one in gas-phase (Figure 2.1).[9] This means that the rate will be higher with a catalyst.

A catalyst can not alter the thermodynamics of the total reaction. However, it is possible that the formation of another product, Q, is thermodynamically favourable, but the kinetics of this reaction is slower than formation of P. By choice of a suitable catalyst, it is possible to make the new kinetics favour Q to P. This property, shown in Figure 2.2, is called *selectivity*.[9]

In order for a catalytic reaction to occur, the reactants, intermediates and products must not bind too strongly nor too weakly to the catalyst. If they adsorb too weakly, they will not be able to adsorb or react on the surface. If they bind too strongly, they will break the catalytic cycle by physically blocking new reactants from reaching the active sites (*poisoning* the surface). This is called the *Sabatier principle*.[36] Assuming that adsorption and desorption are governing the reaction rate, the catalytic rate can be plotted as a function of bond strength limited by two linear equations, corresponding to adsorption and desorption limitation, respectively. In addition to these, constraints related to reaction thermodynamics and kinetics can be added. Such a plot, as seen in Figure 2.3, may often be referred to as a *volcano plot* because of this shape.[9]

As a catalyst is not consumed in the catalytic cycle, by definition, it should have infinite lifetime. In practice, catalysts deactivate over time for a number of reasons.[37] These

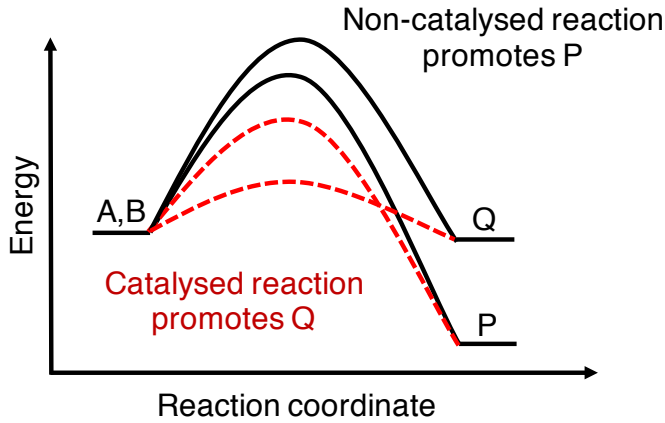

Figure 2.2: Example of a catalyst changing the selectivity from product P to product Q by altering the relative barrier heights. Non-catalysed reaction are in black and catalysed in red.

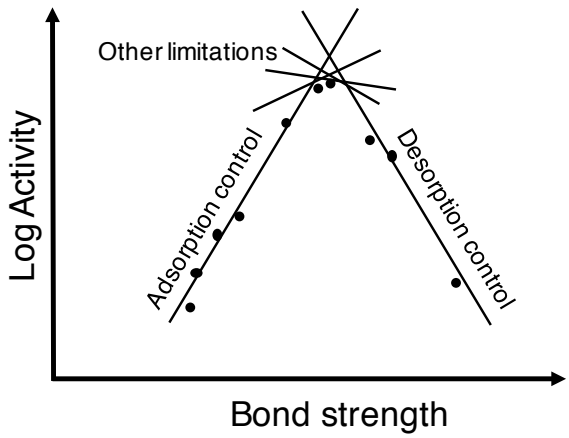

Figure 2.3: The Sabatier principle as a volcano plot. The catalytic activity is limited by bond strength to reactants and products. The highest activity is obtained with a catalyst that neither binds to strongly or to weakly to the adsorbents. There are other thermodynamic and kinetic limitations, which can have impact when the optimal bond strength is achieved.

can be more related to the reaction, such as poisoning the active sites by intermediates or byproducts, or physically blocking the surface (fouling). Processes can also decrease the surface area, e.g. by changing the surface composition, or by coalescing smaller particles to larger (sintering). It is also possible for the surface to suffer mass loss. Thus, *stability* is an important property for a real catalyst.[9] Stability in electrocatalysis differs from other branches of catalysis, since it is the electric potential that makes the system reactive, while temperature and pressure are relatively low (normally limited by the constraints of an aquatic environment).

There are three large classes of catalysis – biocatalysis, homogeneous catalysis and heterogeneous catalysis.[9] Biocatalysts, i.e. enzymes protein synthesis, uses its geometric structure to facilitate a reaction. Homogeneous and heterogeneous catalysts typically have a more specific active site, consisting of few or single atoms; the difference lies in the phases of the catalyst and the reactants. In homogeneous catalysis, they are in the same phase, typically liquid phase. In heterogeneous catalysis, the catalyst is in one phase (typically solid) and reactant are in a different phase (gas or liquid). Electrocatalysis falls within the latter category, since the reactants are dissolved in the electrolyte and the catalytically active electrodes are solid.

2.2 Electrochemistry

Electrochemical reactions are chemical processes that involve charge transfer across an interface between a solid and a liquid phase.[13] Electric potential can be used to drive the reaction, which is called electrolysis, e.g. splitting of water to hydrogen and oxygen and glycerol and methanol electrooxidation. Alternatively, electric power can also be generated by the reaction, which is the case in a galvanic cell, e.g. batteries, and metal corrosion.

The electrochemical cell, as described in the introduction and shown in Figure 1.1, has two electrodes – the anode and the cathode – connected with wires conducting electrons and an electrolyte conducting ions. Reduction reactions (where electrons are gained) occur at the cathode, and oxidation reactions (where electrons are lost) occur at the anode[1]. The pair of reactions are called half reactions, since they must occur simultaneously owing to charge conservation. As an example, we have water splitting,

$$2\,H_2O \longrightarrow 2\,H_2 + O_2, \tag{2.4}$$

where the cathodic half reaction is HER,

$$2\,H^+ + 2\,e^- \longrightarrow H_2 \tag{2.5}$$

and the anodic reaction reaction is the oxygen evolution reaction (OER)

$$H_2O \longrightarrow 2\,H^+ + 2\,e^- + \frac{1}{2}O_2. \tag{2.6}$$

[1]There is a misconception that the anode is always at a higher potential than the cathode. This is true for an electrolytic cell, but it is the opposite in a galvanic cell. In both cases, the electrons flow from the anode to the cathode, but in the galvanic case spontaneously (towards the positive cathode) and in the electrolytic case forcibly.

The anode and cathode half reactions can in many respects be treated separately. For example, the products from water splitting, H_2 and O_2, can be collected without mixing at the cathode and anode side, respectively. This is a general and practical feature for electrochemical reactions.

2.2.1 Nernst equation

We consider the total electrochemical reaction to occur in an isothermal-isobaric ensemble with constant temperature T, pressure p and number of particles N. The thermodynamical potential in this ensemble is the Gibbs free energy, G, with the differential

$$\mathrm{d}G = V\,\mathrm{d}p - S\,\mathrm{d}T - \mathrm{d}W_{\mathrm{el}} \tag{2.7}$$

where V is the volume, S the entropy and W_{el} the electric work.[38] As the pressure and temperature are constant, we see that the difference in Gibbs free energy equals the electric work. The work can be simply derived as the energy gained or lost by moving n_e electrons with charge e over the electric potential U measured vs. a reference potential,[13] meaning that

$$\Delta G = -n_e e U. \tag{2.8}$$

The Gibbs free energy for species i in a mixture is dependent on the thermodynamic activity a_i

$$G_i = G_i^0 + k_{\mathrm{B}} T \ln a_i \tag{2.9}$$

where the superscript 0 denotes a standard state.[13] The activity can be seen as an 'effective concentration'; in the dilute limit, they are equal, but with increasing concentration, the interactions between the particles lowers their ability to be chemically active. In practical calculations, the activity is commonly approximated by properly normalised concentrations.

Inserting Equation 2.8 in Equation 2.9 gives

$$U_i = U_i^0 + \frac{k_{\mathrm{B}} T}{n_e e} \ln a_i \tag{2.10}$$

which is known as the Nernst equation.[39] In principle, U_i can be defined anywhere in the cell, but it is not possible to directly measure the potential in the electrolyte. The reason for this is that there will be an accumulation of charges at the phase barrier between an electrode, including any solid conductor measuring device, and the electrolyte. This is known as the *double layer* and is outlined in Section 2.2.3. As a consequence, it is only possible to measure the potential difference between the metal electrodes.

2.2.2 Reference electrodes

By using a known equilibrium reaction, it is possible to construct a reference electrode. All other reactions can then be defined relative to the reference. Historically, the normal hydrogen electrode (NHE) have been used as a reference potential, defined as the equilibrium for hydrogen gas and free protons and electrons

$$\mathrm{H_2} \longleftrightarrow 2\,\mathrm{H^+} + 2\,\mathrm{e^-}, \tag{2.11}$$

on platinum in a 1 N acid solution (i.e. 1 M H^+ or pH 0) at 1 atm and 298 K.[40] The reason for this definition is that it is easy to construct such an electrode in practice. Later, it has been viewed as more suitable to have a reference where the thermodynamic activity of the hydrogen ions is 1 (i.e. they do not interact with other ions). The latter is known as the standard hydrogen electrode (SHE).[2] Such an electrode can not be constructed, but it can be used as basis for tables on electrodes.

When hydrogen evolution or oxidation half reactions (Equation 2.11) are involved in the total reaction, the electrode potential depends on pH, since hydrogen concentration is included in the Nernst equation. The potential shift,

$$\Delta U = -\frac{k_\mathrm{B}T}{e}\ln[\mathrm{H}^+] = +\frac{k_\mathrm{B}T}{e\ln 10}\mathrm{pH}, \tag{2.12}$$

may be included in the potential itself,[3] which defines the reversible hydrogen electrode (RHE),[41]

$$U_\mathrm{RHE} = U_\mathrm{SHE} + \frac{k_\mathrm{B}T}{e\ln 10}\mathrm{pH}. \tag{2.13}$$

In electrochemical reactions in water, the surface coverage of *O, *OH, and *H is only dependent on potential vs. RHE, regardless of pH, which allows the construction of one-dimensional surface Pourbaix diagrams outlined in Chapter 4. Furthermore, the thermodynamics of e.g. glycerol and methanol deprotonations are only dependent on RHE.

2.2.3 The double layer

Naively, one might think that the potential drops linearly through the electrolyte. However, almost the entire potential drop occurs close to the electrodes in the thin *double layer*.[13] The name refers to the fact that there is one charged layer in the electrode surface and an opposite charge layer in the adjacent electrolyte, which effectively screens the rest of the cell (Figure 2.4). As the thickness of the layer in the electrolyte is in the order of magnitude of the size of hydrated ions,[4] the local electric field is large. From a modelling perspective, this means that the local properties of the double layer, e.g. the electric constant of water,[45] are hard to determine and can not be expected to be similar to the ones in the bulk solution.

On a more macroscopic level, the double layer can be seen as a plate capacitor with a differential capacitance

$$C_d = \frac{\mathrm{d}Q}{\mathrm{d}U} \tag{2.14}$$

where Q is the charge in either of the layers and U is the potential between the electrode and the electrolyte.[13] In an experiment where the potential is varied, (i.e. cyclic voltammetry, section 2.3), a current is generated from the charging and discharging of the double layer.

[2] SHE also differs from NHE that the former is defined at 1 bar = 10^5 Pa, slightly lower than 1 atm, but this is generally negligible.

[3] At room temperature, this shift is 0.059 V per pH.

[4] A Debye length of 3 Å appears in some modelling papers.[42–44] This is the distance after which the potential is decreased by a factor of $1/e$.

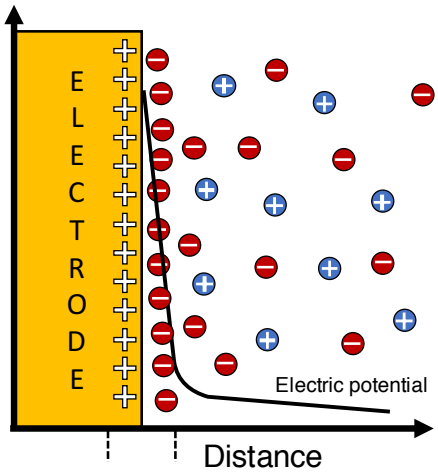

Figure 2.4: The potential difference between the electrode and the electrolyte forms a layer of opposite charges, the double layer, in each medium at the interface. This screens the electric potential effectively, so that almost the entire potential drop takes place there. The figure adapted from Wikimedia Commons.[46]

2.2.4 Kinetics

Consider the Arrhenius equation for the backward and forward rates of an equation with only one step,[13, 47]

$$r = r_+ - r_- = A_+ c_{\text{reac.}} e^{-\beta G_{A,+}} - A_- c_{\text{prod.}} e^{-\beta G_{A,-}}. \tag{2.15}$$

The current i, as well as the forward and backward currents i_+ and i_-, are proportional to the rates with a factor $n_e e$. At the equilibrium potential, U_0, the forward and backward currents are equal. The exchange current density, i_0, is defined as this current,

$$i_0 = i_+(U_0) = i_-(U_0). \tag{2.16}$$

At other potentials there will be a net current in either direction. We define the overpotential[5] as

$$\eta = U - U_0. \tag{2.17}$$

Remember that the thermodynamics of the initial and final states of the reaction changes linearly with the electric potential. This change, $\Delta G = -n_e e \eta$, is added to the difference between the reaction barriers, see Figure 2.5. We introduce a transfer coefficient, $0 \leq \alpha \leq 1$ such that

$$\Delta G_+ = \Delta G_{+,0} - \alpha n_e e \eta \tag{2.18}$$

[5]The term overpotential is sometimes colloquially used for the limiting potential relative to the equilibrium potential, see below.

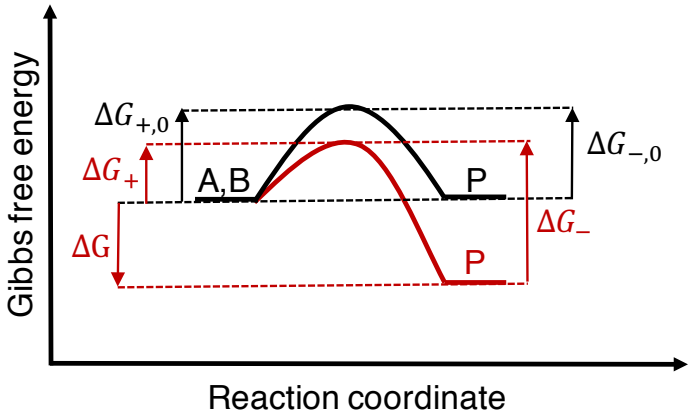

Figure 2.5: Energy landscape of a reaction at the equilibrium potential (black) and a more oxidative potential (red). The change in Gibbs free energy, ΔG, is equal to the barrier difference, $\Delta G_+ - \Delta G_-$.

and

$$\Delta G_- = \Delta G_{-,0} + (1-\alpha) n_e e \eta. \tag{2.19}$$

Thus we have an expression for the total current,

$$i = i_0 \left(e^{\alpha \beta n_e e \eta} - e^{-(1-\alpha)\beta n_e e \eta} \right) \tag{2.20}$$

which is known as the the Butler-Volmer equation. When going to overpotentials far from 0, and as long as the reaction is not limited by transport processes, one of the terms can be neglected, which gives a linear relationship with the logarithm of the current,

$$\eta = b(\ln i - \ln i_0) \tag{2.21}$$

where

$$b = (\alpha \beta n_e e)^{-1} \tag{2.22}$$

is called the Tafel slope.

We see that the thermodynamic landscape – both the product/reactant energies and the barriers – depend strongly on the potential. This is a difference vis-à-vis surface kinetics in standard catalysis, where temperature is the main driving "force" and where we normally treat the barriers as approximately independent of the temperature. A potential is a far superior driving force compared to temperature – a potential of 0.5 eV corresponds to the thermal energy at 6000 K.

Multi-step reactions

Consider an electrochemical reaction with several steps and let us say that it is an oxidation. At the equilibrium potential between the reactants and the products, U_0, there

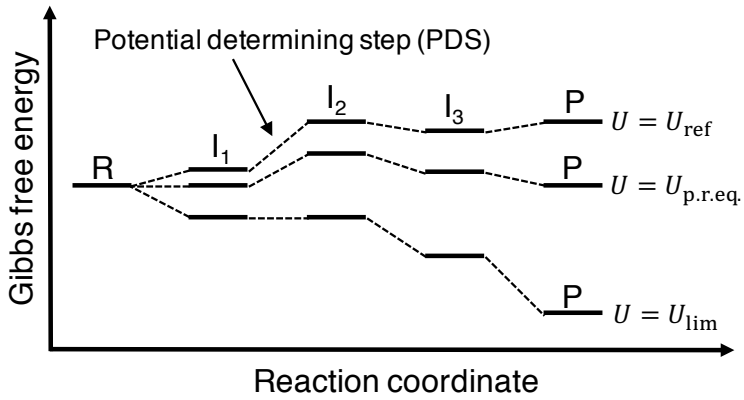

Figure 2.6: Energy landscape of a reaction with four elementary one-electron transfer steps (corresponding to three intermediates). At the reference potential, U_{ref}, some of these steps are uphill and the reaction is not thermodynamically favourable. The largest of these is identified as the PDS. At the product-reactant equilibrium potential $U_{\mathrm{p.r.eq}}$, there are typically still uphill steps, including the PDS. At the theoretical limiting potential, U_{lim}, the PDS is at equilibrium and the reaction is spontaneous. We have $\Delta G_{\mathrm{PDS}} = eU_{\mathrm{lim}}$.

are generally intermediates with lower and higher energy. If we want the forward reaction to be spontaneous, we need to increase the potential until the highest step is energetically 'levelled out', see Figure 2.6. This step is called the *potential determining step* (PDS)[48] and we refer to the associated potential as the *theoretical limiting potential*,[6] U_{onset}, in this thesis.[49] A reaction with several steps has coupled Butler-Volmer equations for every step. Above the theoretical limiting potential, the current is expected to increase more or less exponentially in the kinetic regime. If the PDS is significantly higher than other steps, it can be considered rate-determining, and then the Tafel slope could be associated with it. Regardless, it is not straightforward to find a well-defined onset potential.

In voltammetric experiments, when the potential is swept and the the resulting current is measured, the onset potential is a heuristic concept based on seeing when the reaction visually gets started, rather than rigorous theoretical foundations. There are three common ways of defining an experimental onset potential,[50] as illustrated in Figure 2.7:

a) The potential at which the current exceeds a critical value, i_{crit}.

b) The potential at which the slope, $\mathrm{d}j/\,\mathrm{d}U$ exceeds a critical value.

c) The potential at which the tangent to the curve at the maximum slope of $i(U)$ intersects $i = 0$.

In this project, we are trying to verify calculated limiting potentials, so the important concern is to choose a definition that corresponds to the potential where thermodynamics becomes favourable, i.e. the definition of the theoretical limiting potential shown in

[6] We refer to it as theoretical onset potential in **Paper II**.

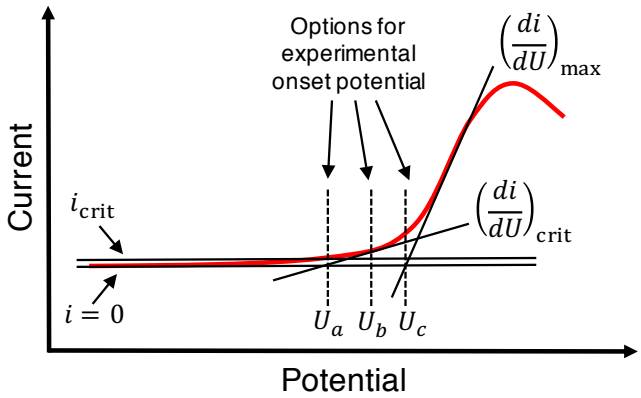

Figure 2.7: Three ways of defining experimental onset potential. a) Critical current. b) Critical slope. c) Tangent intersection. The choice of critical current and critical slope are in principle arbitrary, as long as chosen within reason.

Figure 2.6. Still, we should keep in mind that an experimental onset potential is not an exact value.

Beyond the kinetic regime, the reaction will be limited by transport processes of reactants and products to and from the electrodes. As the focus of this thesis is thermodynamics, only currents near the onset potential are of interest. Thus, we will omit transport processes from this discussion.

2.3 Cyclic voltammetry

Cyclic voltammetry (CV) is a measurement technique, where the potential in an electrochemical cell is varied forward and back between two potentials, and the current is measured as output.[13, 51] Figure 2.8 shows a schematic CV setup with three electrodes – a working electrode (WE), a counter electrode (CE) and a reference electrode (RE)[7] – connected to a potentiostat, operating as an adjustable power source, a voltmeter, and an ammeter. The source potential, U_s, is applied between the WE and CE. The potential between the WE and the RE, U_m, is measured with the voltmeter, and is kept at the desired potential variation by adjusting U_s. The current between the WE and the CE is measured with the ammeter. The setup allows the study of the WE only, as the circuit with the RE and the CE makes sure that U_s is large enough, regardless of the choice of CE. In order to study oxidation reactions on gold, a polycrystalline gold WE was used. The cell setup, including a graphite CE and a Ag/AgCl RE, can be seen in Figure 2.9.

We are interested in converting the measured electrode potential to a standard electrode. Because the studied reactions in this work are pH dependent, we choose RHE. The

[7]The reason for terminology is that the working and counter electrodes typically alternate between being anode and cathode, as the potential is changing.

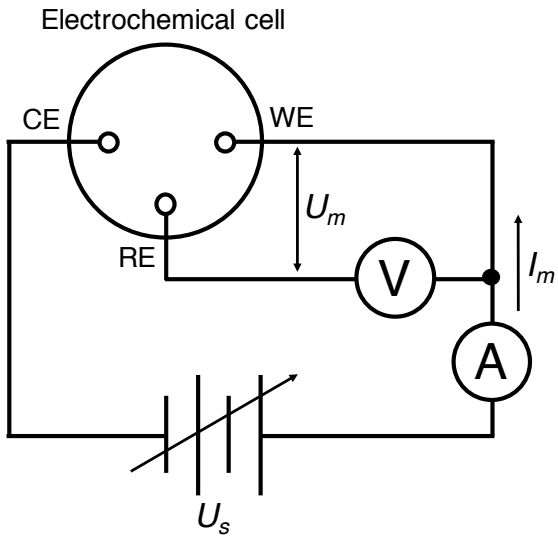

Figure 2.8: Circuit diagram for basic cyclic voltammetry. Adapted from SJ Electronics.[51]

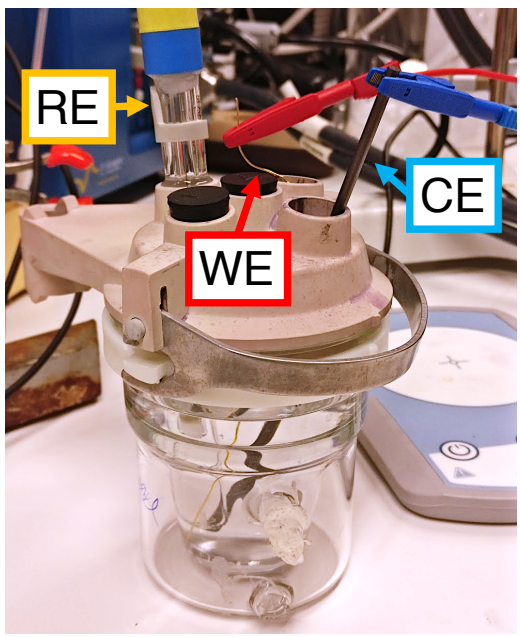

Figure 2.9: Setup of electrochemical cell for cyclic voltammetry. The working electrode (WE) is a polycrystalline gold wire, the counter electrode (CE) a graphite rod, and the reference electrode (RE) Ag/AgCl.

conversion is carried out with the help of the Nernst equation,

$$U_{\mathrm{RHE}} = U_{\mathrm{AgCl},0} + \frac{k_{\mathrm{B}}T}{e}\Big(\ln c_{\mathrm{KCl}} c_{\mathrm{reac.}} + \frac{\mathrm{pH}}{\ln 10}\Big) \tag{2.23}$$

where c_{KCl} is the concentration of KCl in the reference electrode and $c_{\mathrm{reac.}}$ the concentration of (oxidative) reactant, such as glycerol or methanol.

The accuracy of the potentiostat is generally high, in terms of control and sensitivity. However, CV provides no direct information about the cause of the currents. In order to interpret a voltammogram, one must be able to recognise features that are not directly related to the studied reaction. Hydrogen evolution starts when going to low (cathodic) potentials and oxygen evolution (OER) starts when going to high (anodic) ones; on gold, HER starts around the equilibrium potential 0 V vs. RHE[52] while OER requires around 0.7 V of overpotential above the equilibrium potential of 1.23 V vs. RHE.[53] Dissolved atmospheric oxygen is reduced below 1.23 V, according to the oxygen reduction reaction (ORR, the backward reaction in equation 2.6), which can be prevented by purging the cell with nitrogen or argon. There will be a latent current, positive on the anodic scan and negative on the cathodic scan, corresponding to capacitive charge and discharge of the of the double layer. Surface oxidation and reduction will give rise to currents on the anodic and cathodic scans, respectively. In order to try to single out the desired reaction, the voltammogram with the reactant is compared to a blank test.

2.3.1 Underpotential deposition of copper (Cu UPD)

If we want to carry out quantitative comparisons of electrocatalysts, we need to determine the surface current density. As CV gives a total current, it is necessary to measure the electrochemically active area of the electrode submerged in the electrolyte. This can be done with underpotential deposition of Cu (Cu UPD).[54]

The equilibrium potential for the reaction

$$\mathrm{Cu} \longleftrightarrow \mathrm{Cu}^{2+} + 2\,\mathrm{e}^- \tag{2.24}$$

is 0.34 V vs. RHE,[13] meaning that Cu ions in the solution will reduce and form metallic Cu in bulk below this potential. However, it is possible to form a monolayer of Cu at a slightly higher potential. Ideally, a cathodic scan will see two distinguished reduction peaks corresponding to these two processes. The total charge of one monolayer of Cu is computed by integration of the first peak (Figure 2.10). The charge can be converted to a surface area, given knowledge of the surface facets.[54]

2.3.2 Product analysis

Even if we know the current density associated with the reaction, the mechanism and products remain unknown. In situ Fourier transform infrared spectroscopy (FTIR) can be used to study adsorbate vibrations on the surface.[55] For products leaving the surface, gas chromatography (GC) and high performance liquid chromatography (HPLC) may be used. These separate gas and liquid products respectively,[56] which are followed by detection processes. While such analysis could be interesting in the future, we have considered it to be out of scope for this mostly theoretical project.

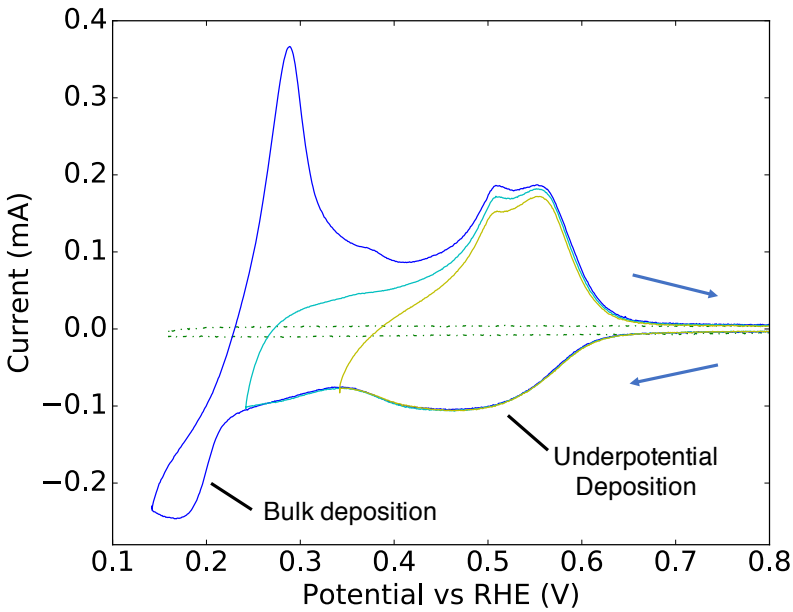

Figure 2.10: Underpotential deposition of copper from supporting information to **Paper II**. As the potential is decreased, a monolayer of Cu forms on the Au surface. Eventually, bulk Cu is deposited (blue). By turning the potential sweep before the bulk deposition (cyan, yellow or somewhere in between), we can measure the deposited and released charge q_{ML} to calculate the surface area. The dotted line is the blank run, dominated by capacitive effects of the double layer.

2.4 Modelling electrocatalysis

We now go to the main task of modelling electrocatalysis on an atomic level. This is carried out with electronic structure calculations in the form of density functional theory (DFT), which is described in detail in Chapter 3. DFT is a common tool for computational catalysis in general. However, in comparison to "standard" computational catalysis, the field of computational electrochemistry is young and in development, in particular with regards to kinetics.

2.4.1 Thermodynamics

Let us assume that we want to model the free energy of the reaction

$$*\mathrm{CHO} \longrightarrow *\mathrm{CO} + \mathrm{H}^+ + \mathrm{e}^-, \tag{2.25}$$

where * stands for an adsorption site. Calculating the energy of the solvated protons and electrons is not easy, but there is a simple way to get around that problem. We know that 0 V vs. RHE is the equilibrium potential for hydrogen protolysis by definition. This means that these systems have the same Gibbs free energy at standard conditions and at this potential. At other potentials, the energy of the proton and electron is shifted with a term $-eU_{\mathrm{RHE}}$. This is known as the *computational hydrogen electrode* (CHE), which was published in 2004 and opened up the field of computational electrocatalysis.[57, 58] Using CHE, under the assumption that the Gibbs free energy of gas-phase hydrogen and the adsorbates are independent of electric potential, we know the reaction free reaction energy (Figure 2.11).

A common, first approximation of calculating the adsorption energies in equation 2.25, is to have the species adsorbed on an extended surface slab, surrounded by vacuum. Even though this is far from realistic reaction conditions, it has been used successfully to understand electrochemical reactions, in particular in regard to trends.[59–62] This is the approach that is used for glycerol oxidation in this thesis.

Solvent effects

Disregarding double-layer effects, adding water molecules or even several water layers can change the difference in binding energy with as much as 0.5 eV between more hydrophilic groups, such as *OH, and *H or *O.[63] There are many ways of introducing water, e.g. ice-like structures. However, if such an ordered structure is used, it may only fit specific facets and unit cells.[64] Furthermore, it is computationally expensive, especially if not an ordered structure is used, meaning that molecular dynamics will be required to get statistics.[64] One hydrogen bond in the water network can correspond to several tens of eV difference. A simple solvent model is the inclusion of one or a few solvent molecules to satisfy bonding to the species, in particular hydrogen bonds; this is known as *microsolvation*.[65]

Implicit solvent models, i.e. considering the solvent as a continuum of dielectrics, are less computationally expensive than explicit solvents.[66] In principle, they can be used on an adsorbate in vacuum, but since the mean field can not represent direct,

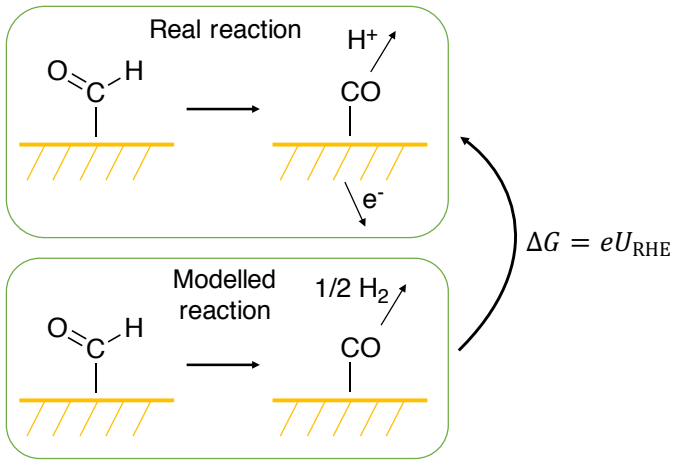

Figure 2.11: Computational hydrogen electrode.

local interaction (such as hydrogen bonds), it is more relevant to use them on top of microsolvated adsorbates.[64] This is used in **Paper V**.

So far, the solvent models have been general and not specific to electrochemistry to handle the double layer. However, there are implicit solvents that can use a Poisson-Boltzmann model to get a potential drop at the surface, such as VASPsol.[67, 68]

Generalised computational hydrogen electrode

So far, we have assumed that the adsorbates are potential-independent, which is normally accurate if the adsorbate is small and does not stretch into the double layer.[69] A consequence of this is coupled proton-electron transfer, which we also have assumed. Adsorbates stretching out into the double-layer region is affected by the environment and will have a potential gradient, which can also decouple the charge transfer. To treat this system, it is necessary to decouple the chemical potential of the protons and electrons through the generalised computational hydrogen electrode (GCHE). This is achieved by calculating the work function, i.e. the difference between the Fermi and vacuum level. Under the assumption that the interface region is charge neutral and large enough to screen all charges, the work function is equal to the absolute electrode potential, for which experimental values range between -4.44 and -4.85 V vs. SHE.[70, 71] It is then necessary to sample the interface region with relevant electrolyte in different structural configurations to vary the work functions and calculate Gibbs free energy at different potentials vs. SHE.[69] This model was considered in this thesis, but it was discarded owing to the observation that the adsorption energy of a probe glycerol intermediate was barely affected by the potential. The reason for this is that few intermediates stretch out from the surface.

2.4.2 Kinetics

When it comes to calculating electrochemical barriers, which are beyond the scope of this thesis, the main issue is that they must be calculated at constant potential. Normally in DFT, the number of charges is constant, which means that the potential can vary by over 2 V between the initial and final state.[72] Surfaces are commonly modelled as periodically repeating supercells, and must be charge neutral. A net charge would mean that the energy of the mirrored electric monopoles goes to infinity.

There are several methods to approach this problem. One way is to calculate the energy barriers with successively larger cells and extrapolate to an infinite cell limit with no potential change.[73, 74] Hydrogen atoms are added or subtracted to control the electric potential. An alternative, less computationally expensive method is to assume that the energy is separable into a "chemical" and a capacitive part, where the latter part is corrected for a posteriori.[72, 75] A third way is varying the number of electrons and compensate with a homogeneous background.[76, 77] Yet another approach is calculating e.g. the H adsorption, using CHE to get the limiting potential for H^+ and e^- to *H, assume that at that potential, the barrier of the reaction $*A + H^+ + e^- \longrightarrow *AH$ is equal to the barrier its corresponding non-electrochemical reaction, and finally using Butler-Volmer theory to generalise to other potentials.[43] A fifth way uses grand-canonical DFT, where the total number of electrons is varied and compensated for in the dielectric continuum of an implicit solvation model, i.e. the electrolyte adjusts to the barrier.[78, 79]

Chapter 3

Density functional theory

> “
> The underlying physical laws necessary for the mathematical theory of a large part of physics and the whole of chemistry are thus completely known, and the difficulty is only that the exact application of these laws leads to equations much too complicated to be soluble.
>
> – Paul Dirac [80]

3.1 From Dirac to Schrödinger

We start our derivation from a relativistic regime (see Strange[81] for further details). The behaviour of quantum mechanical systems is governed by the time-dependent Dirac equation

$$i\hbar\frac{\partial}{\partial t}\Phi(\mathbf{r},t) = \hat{H}\Phi(\mathbf{r},t). \tag{3.1}$$

where the Hamiltonian $\hat{H}$ is a system-dependent operator with real eigenvalues (normally Hermitian), and $\Phi(\mathbf{r},t)$ is the wavefunction, containing all information about the quantum mechanical system.[82] By separation of variables, we assume that the wavefunction can be written as a product of purely time-dependent and a space-dependent parts,

$$\Phi(\mathbf{r},t) = \Psi(\mathbf{r})\chi(t), \tag{3.2}$$

which inserted in equation 3.1 gives

$$\frac{i\hbar}{\chi(t)}\frac{d\chi(t)}{dt} = \frac{1}{\Psi(\mathbf{r})}\hat{H}\Psi(\mathbf{r}). \tag{3.3}$$

As both sides depend only either time or space, they must be constant. It turns out that this constant is the energy, E, so that the time-dependent part, χ can be solved as

$$\chi(t) = e^{\frac{-iEt}{\hbar}} \tag{3.4}$$

and the space-dependent part, Ψ must obey the time-independent Dirac equation,

$$\hat{H}\Psi = E\Psi. \tag{3.5}$$

As we can see, the energies are the eigenvalues of the Hamiltonian. The classical expression of relativistic energy is

$$E = \sqrt{p^2c^2 + m^2c^4}, \tag{3.6}$$

and by insertion of the quantum mechanical operators for momentum, $\hat{\mathbf{p}} = -i\hbar\nabla$, we get the following equation

$$c(-i\boldsymbol{\alpha}\cdot\nabla + \beta mc)\Psi(\mathbf{r}) = E\Psi(\mathbf{r}). \tag{3.7}$$

In order for the square of the right hand side to be equal to the square of the energy, the cross terms must be zero. This means that $\boldsymbol{\alpha}$ and β must be 4×4 matrices, constructed as blocks of 2×2 Pauli matrices and identity matrices. Thus, $\Psi(\mathbf{r})$ is a four-component wavefunction, corresponding to a pair of spinors.

For many elements, in particular gold, relativistic effect are significant, and the full Dirac equation is in principle necessary to solve. The origin of these effects are the relativistic speeds of the core electrons, to which outer electrons respond. By lumping together the core electrons with the nucleus to form an effective potential, a *pseudopotential*, calculations for the valence electrons can be carried out in a non-relativistic scheme.[83, 84]

By rewriting the Dirac equation in the presence of an electromagnetic field, it can be seen that one of the spinors is an order of c smaller than the other one.[1] In the non-relativistic limit, the smaller spinor may be eliminated, and by shifting the the absolute energy with mc^2, we get the (time-independent) Pauli equation,

$$\Big(\frac{1}{2m}\big(-i\hbar\nabla - e\mathbf{A}(\mathbf{r})\big)^2 - \frac{e\hbar}{2m}\boldsymbol{\sigma}\cdot\hat{\boldsymbol{B}}(\mathbf{r}) + V(\mathbf{r})\Big)\Phi(\mathbf{r}) = E\Psi(\mathbf{r}) \tag{3.8}$$

The two components of the wavefunction correspond to spin up and down and are coupled via the magnetic field term. In the absence of magnetic field, the two spin states are no longer coupled and we can reduce the wavefunction to one component. We end up with the familiar time-independent Schrödinger equation,

$$\Big(-\frac{\hbar^2}{2m}\nabla^2 + V\Big)\Psi = E\Psi. \tag{3.9}$$

3.2 The many-body problem

We are considering a system consisting of N electrons with charge e and K positively charged nuclei with charge $Z_I e$. As the potential between two particles with charges q_1 and q_1 is given by the Coulomb interaction

$$V(r) = \frac{q_1 q_2}{4\pi\epsilon_0 r} \tag{3.10}$$

we can write the Hamiltonian as [85, 86]

$$\begin{aligned}\hat{H} = &-\sum_{i=1}^{N}\frac{\hbar^2}{2m_\mathrm{e}}\nabla_i^2 - \sum_{I=1}^{K}\frac{\hbar^2}{2M_I}\nabla_I^2 + \frac{1}{4\pi\epsilon_0}\sum_{i=1}^{N}\sum_{j>i}^{N}\frac{e^2}{|\mathbf{r}_i-\mathbf{r}_j|}\\ &-\frac{1}{4\pi\epsilon_0}\sum_{I=1}^{K}\sum_{i=1}^{N}\frac{Z_I e^2}{|\mathbf{r}_i-\mathbf{R}_I|} + \frac{1}{4\pi\epsilon_0}\sum_{I=1}^{K}\sum_{J>I}^{K}\frac{Z_I Z_J e^2}{|\mathbf{R}_I-\mathbf{R}_J|},\end{aligned} \tag{3.11}$$

[1] For antiparticles, the order of magnitude of the two spinors are opposite, and the energies are negative. Otherwise, the reasoning is analogous.

where m_e and $\mathbf{r}_i$ are the mass and the position of electron i and M_I and $\mathbf{R}_I$ the mass and position of nucleus I. As the particles of the systems are fermions, they cannot occupy the same quantum state according to the Pauli exclusion principle,[87] meaning that the wavefunction must be antisymmetric with respect to exchange of two indistinguishable particles. These constraints, along with the fact that it is a many-body problem, means that the equation is intractable for anything beyond certain one-electron systems, e.g. the hydrogen atom.

3.2.1 Born-Oppenheimer approximation

A first step to reduce the problem is to assume that the electron and ion wavefunctions are separable

$$\Psi_{\text{tot}}(\mathbf{r}, \mathbf{R}) = \Psi_{\text{el}}(\mathbf{r}, \mathbf{R})\Psi_{\text{nuc}}(\mathbf{R}) \tag{3.12}$$

which is known as the Born-Oppenheimer approximation or the adiabatic approximation.[86, 88, 89] The approximation means that the electrons follows the movement of the nuclei instantaneously, while remaining in the same stationary state. The nuclei interacts with an average potential from the electrons and can be treated in a classical, Newtonian fashion. Intuitively, the separation is justified by the fact that the electrons are much lighter than the ions and thus that their time-scales of their dynamics are much smaller. However, this assumes that the energy associated with electron transitions are large enough to keep them in a stationary state. This does not hold for metallic systems, as the electrons have access to a continuum around the Fermi level in response to any nuclear movement. The approximation still holds, however, at temperatures much below the Fermi temperature of the metal (typically thousands of degrees). In this temperature interval, the electron transitions are limited to a small region around the Fermi level, which has little impact of most sought properties.[90] An exception to this is explicit coupled proton-electron transfer in electrochemical kinetics, where non-adiabaticity should be considered.[91, 92]

Under this approximation, the electron Hamiltonian may be written as

$$\hat{H}_{\text{el}} = -\sum_{i=1}^{N} \frac{\hbar^2}{2m_e}\nabla_i^2 + \frac{1}{4\pi\epsilon_0}\sum_{i=1}^{N}\sum_{j>i}\frac{e^2}{|\mathbf{r}_i - \mathbf{r}_j|} - \frac{1}{4\pi\epsilon_0}\sum_{I=1}^{K}\sum_{i=1}^{N}\frac{Z_I e^2}{|\mathbf{r}_i - \mathbf{R}_I|}. \tag{3.13}$$

and by denoting the last term as $V_{\text{ext}}(\mathbf{r}_i)$ and using Hartree atomic units ($\hbar = m_e = e = 1/(4\pi\epsilon_0) = 1$), we have

$$\hat{H}_{\text{el}} = -\frac{1}{2}\sum_i \nabla_i^2 + \sum_i\sum_{j>i}\frac{1}{|\mathbf{r}_i - \mathbf{r}_j|} + \sum_i V_{\text{ext}}(\mathbf{r}_i). \tag{3.14}$$

The many-electron problem still remains intractable. There are essentially two ways to move forward. One way is to expand the wavefunction; the simplest way is to assume that it may be written as a linear combination of products of one-electron wave functions that satifies the antisymmetry property. This approach is called Hartree-Fock and was an early practical method for electronic structure calculations.[86, 93, 94] However, it is

computationally expensive, in particular for larger systems with more than a couple of hundred electrons.

The other approach is to abandon the search for the wavefunction and instead work with the total electron density.

3.2.2 The Hohenberg-Kohn theorems

Using the electron density, $n(\mathbf{r}) = |\Psi|^2$, instead of the wavefunction to evaluate quantum mechanical properties would at least in a formal sense lower the degrees of freedom of the system. This idea was introduced independently by Thomas and Fermi in 1927, [85, 95, 96] but the theoretical framework to justify the approach was put forward in 1964 by Hohenberg and Kohn.[97] The article is the basis for the two Hohenberg-Kohn theorems. The first of these states that the ground state electron density, $n_0(\mathbf{r})$, uniquely determines the external potential. As the many-body Schrödinger equation in principle can be solved knowing V_{ext}, the ground state electron density uniquely defines all the solutions of the wavefunction and thus all properties of the system. The second theorem proves the existence of the universal Hohenberg-Kohn functional $F[n(\mathbf{r})]$ such that the energy functional

$$E[n(\mathbf{r})] = \int V_{\text{ext}}(\mathbf{r}) n(\mathbf{r}) \, \mathrm{d}\mathbf{r} + F[n(\mathbf{r})] \tag{3.15}$$

has its global minimum at the ground state energy, for all possible $V_{\text{ext}}(\mathbf{r})$. However, since we have only rewritten the original problem, finding $F[n(\mathbf{r})]$ would be equivalent to solving the many-body problem and is thus equally intractable.

3.2.3 The Kohn-Sham approach

In 1965, Kohn and Sham proposed a method for handling the universal functional.[90, 98] The idea is to replace the real, interacting electrons with independent particles moving in an effective potential, such that the electron densities are the same. Such Kohn-Sham electrons, with occupied orbitals ψ_i, have the electron density

$$n(\mathbf{r}) = \sum_{i=1}^{N} |\psi_i(\mathbf{r})|^2 \tag{3.16}$$

and kinetic energy[2]

$$T_0 = -\frac{\hbar^2}{2m} \sum_{i=1}^{N} \langle \psi_i | \nabla^2 | \psi_i \rangle. \tag{3.17}$$

A second contribution to the energy comes from the interaction between the electron from the average of all electrons, i.e. from the total electron density. [3] This mean-field

[2] T_0 does not correspond to the real kinetic energy, because the Kohn-Sham orbitals are different from the real ones, even if the electron densities would match.

[3] As the electron density includes the electron in question, this means that E_{H} inherently contains a self-interaction error, which must be taken into account by other means.

Hartree potential V_{H} is calculated from Poisson's equation in classical electrostatics, such that

$$\nabla^2 V_{\mathrm{H}}[n] = -4\pi n(\mathbf{r}). \tag{3.18}$$

From this, we can find the corresponding Hartree energy,

$$\begin{aligned} E_{\mathrm{H}}[n] =& \frac{1}{2}\int V_{\mathrm{H}}[n] n(\mathbf{r})\,\mathrm{d}\mathbf{r} \\ =& \frac{1}{2}\int\int \frac{n(\mathbf{r})n(\mathbf{r}')}{|\mathbf{r}-\mathbf{r}'|}\,\mathrm{d}\mathbf{r}\,\mathrm{d}\mathbf{r}'. \end{aligned} \tag{3.19}$$

The third energy contribution is the interaction between the electron and an external field, V_{ext}, including the potential from the nuclei or pseudopotentials.

These three energy terms are easy to calculate and make up most of the energy. The left-out energy contributions are exchange, which assures that the Pauli principle is upheld, and correlation containing the rest of the many-body effects, including $T - T_0$. In standard DFT, these are lumped together to the exchange-correlation energy E_{xc}. It must be approximated, which is discussed in the next section 3.3. The total energy can now be expressed as

$$E = \int V_{\mathrm{ext}}(\mathbf{r}) n(\mathbf{r})\,\mathrm{d}\mathbf{r} + T_0 + E_{\mathrm{H}} + E_{\mathrm{xc}}. \tag{3.20}$$

By application of the variational principle, we derive the Kohn-Sham equation for electron i,

$$-\frac{1}{2}\nabla^2\psi_i(\mathbf{r}) + \left[V_{\mathrm{ext}}(\mathbf{r}) + \int \frac{n(\mathbf{r}')}{|\mathbf{r}-\mathbf{r}'|}\,\mathrm{d}\mathbf{r}' + \frac{\delta E_{\mathrm{xc}}}{\delta n(\mathbf{r})}\right]\psi_i(\mathbf{r}) = \epsilon_i\psi_i(\mathbf{r}). \tag{3.21}$$

Note that the Kohn-Sham orbitals ψ_i and the Kohn-Sham energies ε_i are not the same as the real orbitals or energies, but only exist to find the true electron density, $n(\mathbf{r})$, and the energy,

$$E[n] = \sum_{i=1}^{N}\epsilon_i - E_{\mathrm{H}}[n] - \int n(\mathbf{r}) V_{\mathrm{xc}}[n(\mathbf{r})]\,\mathrm{d}\mathbf{r} + E_{\mathrm{xc}}[n]. \tag{3.22}$$

A typical DFT implementation solves the Kohn-Sham equations, with an appropriate choice of exchange-correlation functional. Starting with an initial guess of $n(\mathbf{r})$, e.g. a sum of atomic orbitals, the equations are solved iteratively until self-consistency.

Implicit solvation

The Kohn-Sham approach can be modified to include an implicit solvation by introducing a density-dependent permittivity $\varepsilon[n]$ entering a modified Poisson equation. In VASPsol[67, 68], the permittivity changes gradually from 1 to the bulk dielectric constant $\varepsilon_{\mathrm{bulk}}$ (78.4 for water at standard conditions) by having the form

$$\varepsilon[n] = 1 + (\varepsilon_{\mathrm{bulk}} - 1)\zeta[n] \tag{3.23}$$

where $\zeta[n]$ is a cavity shape function. It is given by

$$\zeta[n] = \frac{1}{2}\mathrm{erfc}\left(\frac{\log(n/n_{\mathrm{cut}})}{\sigma\sqrt{2}}\right), \tag{3.24}$$

where n_{cut} determines at what value of the electron density the dielectric cavity forms and σ is the width of the diffuse cavity.

Poisson's equation (Equation 3.18) is modified to include dependence of the permittivity and charges in the dielectric. We have the generalised Poisson-Boltzmann equation,

$$\nabla \cdot (\varepsilon \nabla V_{\mathrm{H}}) = -4\pi(n + n_{\mathrm{ion}}), \tag{3.25}$$

where n_{ion} is the density of the electrolyte. After several approximations, such as negligible ion-ion interaction, that the cations and anions have equal and opposite sign, that the electrostatic potential in the electrolyte region is small, and that the ions are treated as point charges, Equation 3.25 can be linearised to

$$\nabla \cdot (\varepsilon \nabla V_{\mathrm{H}}) - \frac{\zeta}{\lambda_{\mathrm{D}}} V_{\mathrm{H}} = -4\pi n, \tag{3.26}$$

where λ_{D} is the Debye length, i.e. the length where the potential has decayed exponentially with a factor of $1/e$.

In addition to the changes to the Kohn-Sham equations, when calculating the Helmholtz free energy described in Chapter 4, terms for the ions,

$$F_{\mathrm{ion}} = k_{\mathrm{B}} T S_{\mathrm{ion}}, \tag{3.27}$$

where S_{ion} is the entropy of mixing of the electrolyte ions, and for cavities,

$$F_{\mathrm{cav}} = \tau \int |\nabla \zeta| d\mathbf{r}, \tag{3.28}$$

where τ is an empirically optimised parameter, must be added.

3.3 Exchange-correlation functional

The exact exchange-correlation functional is not known, and, as finding it would be at least as hard as solving the classical many-body problem. We are left with using different levels of approximations, which can be ordered on the so-called Jacob's ladder from the Hartree world to the heaven of chemical accuracy.[99] Climbing higher on the ladder increases computational costs and, hopefully, increases accuracy.

A natural starting point for approximations is the homogeneous electron gas, which is a decent model for metallic systems. The exchange energy, ϵ_{x}, is given exactly as[90]

$$\epsilon_{\mathrm{x}}^{\mathrm{h}}[n] = -\frac{3}{4}\left(\frac{3n}{\pi}\right)^{\frac{1}{3}} \tag{3.29}$$

while the correlation energy, $\epsilon_{\mathrm{C}}^{\mathrm{h}}$, has been computed with Monte Carlo simulations to high numerical accuracy.[100] With help of this, and assuming that the electron density behaves

locally as the homogeneous electron gas, we can make approximations of the exchange-correlation functional for a general system by expansion in terms of the derivatives of the electron density.

The first approximation is the local density approximation (LDA),[98] which locally only depends on the value of $n(\mathbf{r})$. We have

$$E_{\mathrm{xc}}^{\mathrm{LDA}} = \int n(\mathbf{r})\epsilon_{\mathrm{xc}}^{\mathrm{h}}[n(\mathbf{r}), \mathbf{r}]\,\mathrm{d}\mathbf{r}. \tag{3.30}$$

Usually, the accuracy provided by LDA is not enough. The next rung of the ladder is to add dependence of the gradient of $n(\mathbf{r})$, in the generalised gradient approximation (GGA)[101–104]

$$E_{\mathrm{xc}}^{\mathrm{GGA}} = \int n(\mathbf{r})\epsilon_{\mathrm{xc}}^{\mathrm{h}}[\nabla n(\mathbf{r}), n(\mathbf{r}), \mathbf{r}]\,\mathrm{d}\mathbf{r}. \tag{3.31}$$

A relatively computationally cheap and overall accurate GGA functional was introduced by John Perdew, Kieron Burke, and Matthias Ernzerhof in 1996.[105] These qualities, together with it being a relatively simple description, has made the PBE functional one of the most popular choices of exchange-correlation functional. However, PBE has a number of drawbacks in terms of accuracy for certain systems; a particular case in this project is its lack of long-range dispersion, which is discussed below. In addition to PBE, there are a number of other GGA functionals. Some of them have been developed addressing the shortcomings of PBE on a more rigorous level, while others have been fitted to chemical data.

The third rung of the ladder includes dependence on the second derivative of the electron density, $\nabla^2 n(r)$, which can be interpreted as the kinetic energy of the Kohn-Sham electrons. [106] This is called Meta-GGA.

On any level on Jacob's ladder, it is possible to improve accuracy by including exact exchange, i.e. perfect obedience to the Pauli exclusion principle for fermions. Exact exchange is obtained from Hartree-Fock theory, which is a wavefunction based theory. In practice, hybrid functionals are constructed by calculating Hartree-Fock exchange for the Kohn-Sham orbitals, which is mixed into the rest of the DFT solution.[107] These can calculate e.g. band gaps accurately, but are very computationally expensive.[108]

3.3.1 Long range dispersion

Exchange-correlation functionals in the lowest steps of Jacob's ladder are local or semi-local in nature, and can not model long range effects.[109] In particular, London dispersion forces between instantaneous multipoles, stemming from quantum fluctuations,[4][110] are missed out.[111] There are several approaches to add dispersion to GGA functionals:

A simple model, proposed by e.g. Grimme,[112] is to parametrise the interaction by introducing pairwise terms, proportional to $1/r^6$ at medium to large distances, similar to the Lennard-Jones potential.[113] However, the approximation that the total interaction

[4]London dispersion is some times used interchangeably with van der Waals. Strictly speaking, van der Waals includes London dispersion, as well as e.g. interactions between permanent dipoles, and permanent-induced dipole pairs.

can be obtained by summing of pair potentials is inaccurate for many systems, as a third (forth, fifth etc.) atom influences the dynamic multipoles in the pair.[114]

Lundqvist et al.[115, 116] put forward the idea of calculating the total correlation as the sum of a local and a non-local contribution

$$E_{\mathrm{c}} = E_{\mathrm{c}}^{\mathrm{l}} + E_{\mathrm{c}}^{\mathrm{nl}}, \tag{3.32}$$

where $E_{\mathrm{c}}^{\mathrm{l}}$ is approximated as the LDA correlation and

$$E_{\mathrm{c}}^{\mathrm{nl}} = \frac{1}{2}\int n(\mathbf{r})\phi_k(\mathbf{r},\mathbf{r}')n(\mathbf{r}')\,\mathrm{d}\mathbf{r}\,\mathrm{d}\mathbf{r}', \tag{3.33}$$

where ϕ_k is a generating response function known as the kernel. The choice of exchange fell on a variant of PBE (revPBE)[117], and this functional is called vdW-DF.[116] By instead choosing fitted exchange proposed by Becke,[102, 118, 119] Klimeš et al. developed the optB88-vdW and optB86b-vdW.[120, 121] Another variety is to use training on chemical data sets with machine learning to get a bayesian error estimation functional (BEEF-vdW).[122]

3.3.2 Spin

In order to model magnetic and open shell systems correctly, we need to include spin. From the Pauli equation (Equation 3.8), we know that the wavefunction in the non-relativistic regime is a two-component spinor coupled with the magnetic field. In the Kohn-Sham approach (equation 3.20) we see that the kinetic energy, depending on ψ_i, is trivially split into the two components, while the external and Hartree potentials only depend on the total electron density. The coupling is therefore contained in the exchange-correlation functional,

$$\epsilon_{\mathrm{xc}} = \epsilon_{\mathrm{xc}}[n_\uparrow, n_\downarrow], \tag{3.34}$$

which would mean that the generalisation in the case of LDA, the local spin density approximation (LSDA),[123, 124] would be

$$E_{\mathrm{xc}}^{\mathrm{LSDA}}[n_\uparrow, n_\downarrow] = \int \Big(n_\uparrow(\mathbf{r}) + n_\downarrow(\mathbf{r})\Big)\epsilon_{\mathrm{xc}}^{\mathrm{h}}[n_\uparrow(\mathbf{r}), n_\downarrow(\mathbf{r}), \mathbf{r}]\,\mathrm{d}\mathbf{r}. \tag{3.35}$$

$\epsilon_{\mathrm{xc}}^{\mathrm{h}}$ would in this case be a linear combination of exchange-correlation for fully polarised and unpolarised homogeneous electron gas. The spin versions of GGA and higher exchange-correlation functions are found in an analogous fashion.

3.4 Hellmann-Feynman theorem

If the Hamiltonian depends on a parameter λ, we have[125]

$$\frac{\mathrm{d}E_\lambda}{\mathrm{d}\lambda} = \langle\Psi_\lambda|\frac{\partial\hat{H}_\lambda}{\partial\lambda}|\Psi_\lambda\rangle. \tag{3.36}$$

which is known as the Hellmann-Feynman theorem. A special case of λ of interest is the coordinate of nucleus I, $\mathbf{R}_I$. This derivative will give us the force on nucleus I. From the many-body Hamiltonian (equation 3.11), and under the Born-Oppenheimer assumption that the nuclei interact with the average of the electron cloud, we get

$$\begin{aligned} -\frac{\partial E}{\partial \mathbf{R}_I} &= \langle \Psi | - \frac{\partial \hat{H}}{\partial \mathbf{R}_I} | \Psi \rangle \\ &= \int n(\mathbf{r}) \frac{Z_I(\mathbf{r} - \mathbf{R_I})}{|\mathbf{r} - \mathbf{R}_I|^3} \mathrm{d}\mathbf{r} + \sum_{J \neq I} \frac{Z_I Z_J (\mathbf{R}_I - \mathbf{R}_J)}{|\mathbf{R}_I - \mathbf{R}_J|^3} \end{aligned} \tag{3.37}$$

which is the same as the classical expression. For practical purposes, this means that both the energy and the force can be calculated in a single-point calculation.

3.4.1 Second derivative

The Hellmann-Feynman theorem can in principle be extended to the second derivative of a parameter, namely [126, 127]

$$\frac{\mathrm{d}^2 E_\lambda}{\mathrm{d}\lambda^2} = \langle \Psi_\lambda | \frac{\partial^2 \hat{H}_\lambda}{\partial \lambda^2} | \Psi_\lambda \rangle + 2 \langle \frac{\partial \Psi_\lambda}{\partial \lambda} | (E_\lambda - \hat{H}_\lambda) | \frac{\partial \Psi_\lambda}{\partial \lambda} \rangle. \tag{3.38}$$

However, it is not possible to calculate the second term in standard DFT, since the wave function and its derivatives are not directly accessible. Instead, the second derivative with respect to nuclear coordinates (the Hessian matrix) can be calculated numerically with finite differences, or analytically with more complex methods, such as the coupled-perturbed Kohn-Sham method,[128] the fragmented molecular orbital method,[129] and auxiliary density pertubation theory.[130]

3.5 Basis sets and periodicity

When solving the Kohn-Sham equations computationally, the orbitals must be expanded in a basis set χ_j

$$\psi_i = \sum_j^K c_{ij} \chi_j, \tag{3.39}$$

where the size of the basis set, K, in principle is infinite, but limited in practical application.[86] Insertion in equation 3.22,

$$\sum_j c_{ij} \hat{H} | \chi_j \rangle = \varepsilon_i \sum_j c_{ij} | \chi_j \rangle, \qquad i = 1, 2, 3, \ldots, N, \tag{3.40}$$

and multiplying with the complex-conjugate $\langle \chi_k |$, we obtain

$$\sum_j c_{ij} \langle \chi_k | \hat{H} | \chi_j \rangle = \varepsilon_i \sum_j c_{ij} \langle \chi_k | \chi_j \rangle, \qquad i = 1, 2, 3, \ldots, N. \tag{3.41}$$

Introducing the shorthand notation $H_{kj} = \langle \chi_k | \hat{H} | \chi_j \rangle$, $S_{kj} = \langle \chi_k | \chi_j \rangle$ and omitting the i in the coefficients, we have

$$H_{kj} C_j = \varepsilon_i S_{kj} C_j, \qquad i = 1, 2, 3, \ldots, N, \quad k = 1, 2, 3, \ldots, K, \tag{3.42}$$

which may be written on matrix form as

$$(\mathbf{H} - \varepsilon_i \mathbf{S})\, \mathbf{C} = \mathbf{0}, \qquad i = 1, 2, 3, \ldots, N. \tag{3.43}$$

This is a generalised eigenvalue problem for ε_i with the Hamiltonian matrix $\mathbf{H}$, the overlap matrix $\mathbf{S}$ and the basis coefficient vector $\mathbf{C}$.

3.5.1 Plane-waves and pseudopotentials

A natural choice of basis set for a periodic system is plane-waves.[85] Since plane-waves are orthogonal, the overlap matrix $\mathbf{S}$ reduces to the identity matrix. In the work presented here, the plane-wave based Vienna Ab-initio Simulation Package (VASP)[131, 132] was used for all calculations. The Kohn-Sham orbitals are expanded in a Fourier series

$$\psi_i = \sum_{\mathbf{k}} c_{i\mathbf{k}} e^{i\mathbf{k}\cdot\mathbf{r}}, \tag{3.44}$$

where the i in the exponent is the imaginary number. The series is truncated so that the kinetic energy of the plane-waves are smaller than a cut-off energy, i.e.

$$\frac{\hbar^2 k^2}{2m_e} < E_{\text{cut}}. \tag{3.45}$$

When a low cut-off is used, only smooth changes of the orbitals are accurately described. Including higher wave numbers will describe more rapid features and ultimately converge more or less monotonically. Rapidly changing core electronic orbitals are hard to converge, but it can be avoided by combining the plane-wave basis set with pseudopotentials. Performing calculations only for the valence electrons is often an acceptable approximation, as their behaviour is normally what decides the chemical properties of an atomic system. All-electron calculations require in general that relativistic effects are accounted for in some way, as mentioned in Section 3.1.

K-point sampling and smearing

Working with a periodic system, it is natural to Fourier transform it to perform calculations in reciprocal space (k-space). Implementation of the Kohn-Sham integrals is carried out as a summation over well chosen k-points.[133] The discrete nature of the k-point sampling can lead to a convergence problem: An electron close to the Fermi level can in one iteration be placed in one orbital, which in turn changes the electron structure. The new electron structure makes it beneficial for the electron to move to a new orbital, which gives the original (or similar) electron structure. A remedy to this oscillatory behaviour is electron smearing, i.e. allowing partial occupation of orbitals.[134] One example is to let the electrons be Fermi-Dirac distributed at a fictive electron temperature greater than zero. Once the system has converged, the energy is extrapolated back to 0 K.

Chapter 4

Applied electronic structure calculations

> “
> Knowing is not enough; we must apply. Willing is not enough; we must do.
>
> – Johann Wolfgang von Goethe

The use of electronic structure calculations, allows us to calculate the energy of a system of atoms for a certain geometry. However, these absolute energies are not very useful in isolation. We can get around this by instead calculating differences of total energies. From this, we can determine physical properties, such as adsorption sites, adsorption energy, spectroscopic vibration energies and reaction free energy, through methods such as energy optimisation, vibrational analysis, and thermodynamics.

4.1 Finding minima

Most properties we are interested in are calculated in an energetically local minimum, i.e. a configuration where any displacement results in a higher energy. To find a local minimum, we need to determine the forces along each coordinate,

$$f_i = \frac{\partial E}{\partial R_i} \tag{4.1}$$

and follow the gradient until the norm of each f_i is below a certain limit, e.g. $0.02\,\mathrm{eV/Å}$.[86] This process is called *relaxation*. The fact that the force can be evaluated for each single point calculation simplifies the process.

Relaxations will only find the closest minimum, and if the starting configuration is far from this minimum, a lot of computational time will be wasted. It is often worthwhile to use chemical intuition to guess reasonable starting configurations. However, there is a balance between guessing and letting the computer cluster work.

Molecular dynamics is a method that can be used to sample configuration space to find minima.[135] It lets the system evolve in time in thermodynamic ensembles, such as the microcanonical ensemble with energy, temperature, and number of particles fixed. As our relevant reaction conditions have constant temperature, we prefer to have an isothermal system, which requires a thermostat. Temperature corresponds to the kinetic energy of the atoms, which is non-trivial to control – just rescaling the velocities at regular intervals does not represent realistic dynamics.[136] We use a Nosé-Hoover thermostat in this work, which involves the interaction of an imaginary particle, whose mass controls the frequency of the temperature oscillations.[137–140]. Ideally, we would like to work in the Gibbs ensemble that also has constant pressure, which is possible by changing the volume of the cell dynamically, but this unnecessarily complicated for the reaction conditions in this work, especially when the intention is to generate starting configuration for relaxations.

4.2 Adsorption and reaction energies

When in a local minimum, we can calculate reaction and adsorption energies as the energy difference between a reference state and a final state. For adsorption of A on top of a surface $*$, three calculations are required: One of A in gas phase (A_g), one with adsorbed A ($A*$) and one with surface only ($*$). The adsorption energy is calculated as

$$E_{\text{ads}}(A) = E_{\text{tot}}(A*) - E_{\text{tot}}(*) - E_{\text{tot}}(A_g) \tag{4.2}$$

With this definition, we have that $E_{\text{ads}} < 0$ means that adsorption is energetically favourable.

A general reaction is calculated in an analogous way, conserving the number of atoms of each element for the initial and final states.

4.2.1 Scaling relations

Transition metals are characterised by having a broad sp-band and a narrow d-band (broad and narrow meaning allowing a large and a small range of energies, respectively) filling up as going from to the right in the periodic table. An adsorbate on such a surface will have similar interactions with the sp-band for all transition metals and the difference in adsorption lies mainly in the interaction with the d-band. Its narrowness means that it forms molecular-like bonding and anti-bonding states with the adsorbate. Depending on the position of the d-band centre and how filled it is, the anti-bonding state may be partly filled, weakening the bond.[141, 142]

An idea that rises from the molecular-orbital-like binding in the d-band model, is that the adsorption is determined by the adsorbate atom(s) binding to the surface, and thus that species binding through the same mechanism, scale with each other. As examples, adsorbed atomic carbon should scale with *CH_3, CH_2OH, and atomic oxygen with *OH and CH_3O*. Abild-Pedersen et al.[142] showed that the adsorption energy for atom A (A = C, O, N, S) scales linearly with the adsorption energy for a species AH_x, ΔE_{AH_x} ΔE_A, such that

$$\Delta E_{AH_x} = \gamma \Delta E_A + \xi, \tag{4.3}$$

where γ and ξ are fitting parameters. The intercept, ξ, corresponds to the constant binding to the sp-band. The slope γ is observed to match the ratio of valencies, v, of the adsorbate, i.e.

$$\gamma = \frac{v_{AH_x}}{v_A} \tag{4.4}$$

which informally can be interpreted as, e.g., a double bond to the surface being twice as strong to a single bond. There are more rigorous investigations on the physics of scaling relations. This is, however, outside the scope of this work, since we restrict ourselves to applying them as a practical tool.

4.3 Vibrational analysis

The molecules and adsorbates of interest vibrate around the energetic minimum found by a relaxation. A way to interpret this is to compare bonds to springs counteracting

displacements from the equilibrium. Calculations of vibrational frequencies are useful to compare with spectroscopic measurements and to calculate thermodynamic properties.

Vibrational frequencies are calculated using the theory of small oscillations.[143] This assumes that the energy landscape is locally harmonic around the equilibrium, which means that the vibration modes can be obtained by diagonalising the mass-weighted Hessian matrix (see Appendix). Classically, these modes can have any energy, but quantum mechanics dictates that only the following energy levels are allowed:

$$E_{m,j} = \left(j + \frac{1}{2}\right)\hbar\omega_i, \qquad m = 0, 1, 2, \ldots \tag{4.5}$$

Not all mathematical solutions from vibrational analysis correspond to true vibrations. A gas-phase species will have three modes corresponding to translation and three corresponding to rotation (two for a linear molecule). These will yield near-zero frequencies (imaginary if the curvature is negative) in the vibrational analysis scheme and must be treated separately.

4.4 Statistical mechanics

In principle, DFT calculations are carried out at 0 K whereas pressure remains somewhat undefined. In order to relate the obtained energies to what can be observed at realistic conditions, we need to use thermodynamics and statistical mechanics.

We consider our surface reactions to occur at the ambient temperature (293 K) and pressure (1 atm). This means that we are in the isothermic-isobaric ensemble, for which the Gibbs free energy is minimised. This is given by

$$G = U_{\text{int}} + pV - TS, \tag{4.6}$$

where U_{int} is the internal energy, p pressure, V volume, T temperature and S entropy. For adsorbates, we consider the small volume changes to be negligible and approximate G with Helmholtz free energy

$$F = U_{\text{int}} - TS. \tag{4.7}$$

For a gas-phase species, we assume the ideal gas approximation, where

$$V = NRT/p. \tag{4.8}$$

In both these cases, we see that we can consider the volume to be constant and make our derivations in the canonical (NVT) ensemble.

For further reading on the derivations below, see Stoltze[144], Chorkendorff and Niemantsverdiet[9], and the documentation for the Atomic Simulation Environment.[145]

4.4.1 Free energy for gas phase species

We start by calculating the internal energy $U_{\text{int},0}$ at 0 K,

$$U_{\text{int},0} = E_{\text{el}} + E_{\text{ZP}}, \tag{4.9}$$

where E_{el} is the DFT energy and E_{ZP} is the zero point correction, which stems from the lowest energy level of the vibrational modes in equation 4.5. This is equal to the Helmholtz free energy at 0 K, F_0. To get F at temperature T, we need to add ΔF, which in the canonical ensemble is simply related to the partition function Z as

$$\Delta F = -k_{\mathrm{B}} T \ln Z. \tag{4.10}$$

The partition function, whose most important contributions are translational, rotational, and vibrational, is derived in Appendix. To the Helmholtz free energy at temperature T, we add a term of electric work,

$$W_{\mathrm{el}} = n_e e U_{\mathrm{RHE}} \tag{4.11}$$

corresponding to the energy gained or lost by moving n_e electrons, with charge e, over the electric potential U_{RHE}. We can also add a term for pressure,

$$\Delta G_p = k_{\mathrm{B}} T \ln \frac{p}{p_{\mathrm{ref}}} \tag{4.12}$$

where p_{ref} is the reference pressure. Finally, as $G = F + pV$ and $pV = k_{\mathrm{B}} T$ for an ideal gas, we simply have

$$G = E_{\mathrm{el}} + E_{\mathrm{ZP}} + k_{\mathrm{B}} T (1 - \ln Z + \ln \frac{p}{p_{\mathrm{ref}}}) - n_e e U_{\mathrm{ref}}. \tag{4.13}$$

4.4.2 Free energy for adsorbates

We consider adsorbates to be fixed at the surface. Treating all degrees of freedom as harmonic vibrations is called the *harmonic approximation.*[146] Furthermore, even if an adsorbate would have an open shell in gas phase, we consider the its spin to be quenched by the sea of free electrons in an extended metallic surface with no net spin. Thus, only the vibrational partition function will give a contribution. We get the approximate Gibbs free energy as

$$G \approx F = E_{\mathrm{el}} + E_{\mathrm{ZP}} - k_{\mathrm{B}} T \sum_m \ln z_{\mathrm{vib},m} - n_e e U_{\mathrm{RHE}}. \tag{4.14}$$

4.5 Applications for electrolysis

4.5.1 Surface Pourbaix diagrams

A Pourbaix diagram is a two-dimensional phase diagram as a function of pH and potential,[13] named after Marcel Pourbaix for his studies of corrosion. The diagram is calculated using thermodynamic data of the material in question and the Nernst equation. However, the diagrams that use tabulated experimental data is normally only valid for the bulk of the material, and we are interested in knowing the local surface structure. Using density functional theory, it is possible to construct a surface Pourbaix diagram by calculating the energy of adsorbed oxo (*O) or hydroxo (*OH) groups.[42, 147] The surface Pourbaix diagram is easy to read since it is one-dimensional, only depending on the potential, since the pH dependence is implicit when using RHE (Figure 4.1).

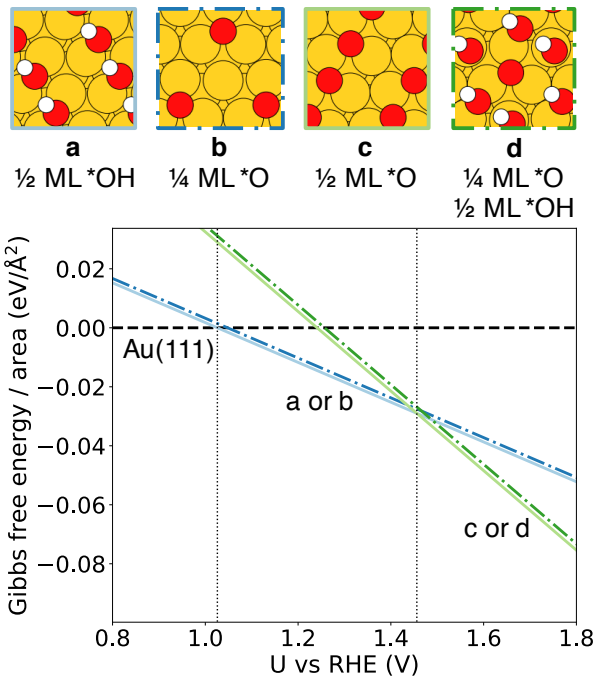

Figure 4.1: Surface Pourbaix diagram of Au(111) calculated in **Paper II**. The surface is adsorbent-free at potentials below 1.0 V vs. RHE, above which (a) 1/2 ML *OH and (b) 1/4 ML *O are formed. At 1.5 V, (c) 1/2 ML *O and (d) a mixture of 1/4 ML *O and 1/2 ML *OH are formed.

Chapter 5

Summary of papers and conclusion

> ”
> An expert is someone who has made all the mistakes which can be made in a narrow field.
>
> – Niels Bohr

When Rudolph Diesel developed his engine in the end of the 19th century, he tested vegetable oils as fuel.[148] From then on, petroleum-derived fuels were mainly used, with exceptions in the 1930s and 1940s when vegetable oils was used as an emergency solution. For many decades, there was no reason to replace petrol, but that changed with the oil crisis 1973–1974, which reignited the research for alternative fuels. It is also at this time the first glycerol electrooxidation experiments were carried out for possible use in fuel cells, along with methanol and other alcohols.[149, 150] The biodiesel industry has grown much since then, owing to environmental concerns. A particular expansion occurred during the mid-2000s when crude oil prices increased a lot,[151] which eventually led to the need for valorisation of its byproduct, glycerol.

The first computational glycerol decomposition studies were carried out in the beginning of the 2010s by Liu and Greeley[152–154] and Chen et al.[155] The reason for the relatively late date is the fact that glycerol is large in a DFT perspective, with a complex and vast amount of possible intermediates and products. Even when the reaction pathways are restricted to dehydrogenation reactions, there are 80 possible intermediates with regards to internal structures, and even more if the several ways of satisfying all bonds are taken into account. Chen et al. and Liu and Greeley used priori methods based on group additivity and scaling relations to decrease the number of necessary calculations.[153, 155] It can be noted that these studies were focused on heterogeneous catalysis, but by using the computational hydrogen electrode, their results can be interpreted in an electrochemical context, which we do extensively.

With this background, the work in the papers are presented.

5.1 Paper I

The first paper covers glycerol adsorption on Au(111), studied with DFT. Structural, electronic, and vibrational properties were investigated on bare and surface-alloyed Au(111). As gold is inert to form formal bonds, adsorption is dominated by dispersion effects, which thus must be modelled accurately. Hence, a number of dispersion-corrected functionals were tested on a model system, methanol adsorbed on gold, to select an appropriate exchange-correlation functional called optB86b-vdW. This selection is then used for later electrooxidation studies.

5.2 Paper II

In the second paper, we calculate full glycerol deprotonation to CO on a Au(111) in a systematic way to determine the reaction mechanism and theoretical limiting potentials. A surface Pourbaix diagram was constructed to verify that the bare Au(111) surface is clean at the calculated theoretical limiting potentials with 0.5 V of margin to partial *OH cover. However, since Kwon et al.[156] had shown that in alkaline solution, glycerol is protolysed in the electrolyte, which changes the adsorption process and potentially the reaction mechanism, we decided to present a study in acidic solution. While previous experimental studies for glycerol electrooxidation on gold in acidic media reported no activity,[157, 158] which is a reasonable statement in comparison to alkaline conditions, we showed experimentally that there is a detectable activity, in particular with the choice of a weakly binding anion (perchlorate).

5.3 Paper III

The third paper is dedicated to electrooxidation on various late transition metals. In general, in contrast to gold, we expect most metals oxidise to get *O or *OH cover of even be oxidised at potentials required for a full deprotonation. In such a case, glycerol intermediates have access to oxygen and deviates from pure deprotonation, which has to many paths to follow. We choose to study the two first dehydrogenation steps on model surfaces, mainly for selectivity, and beyond that connect to experimentally reported reaction mechanisms. In comparison to experiment, however, we find a general preference for oxidation of the secondary group, while experiments indicate that it is often the primary group that is oxidised. Possible explanations are presence of other surface facets in the experiments and that the secondary group has less geometrical access to the surface (steric hindrance).

5.4 Paper IV

In the fourth paper, we establish scaling relations for first and second-dehydrogenated glycerol intermediates with two different pairs of descriptors, *C and *O on one hand $^*CH_2OH$ and CH_3O^* on the other, discussing whether is it worth to use the slightly more complicated descriptors, which are better but somewhat more costly to calculate, in particular since there are lots of data for *O and *C binding energies available in different data bases. We calculate selectivity map as a function of descriptors, which can be used to find alloys or other materials for an optimal electrocatalyst.

5.5 Paper V

The fifth paper investigates the impact of explicit and implicit solvent effects on the methanol electrooxidation landscape on Au(111). We use VASPsol and restrict ourselved to pure solvent effects without electrochemical effects. As explicit solution, we use up

to four water molecules for microsolvation. Molecular dynamics are used to sample the configuration space of these water structures and we average energies over the samplings. We find that the first deprotonation step remains *CH_2OH, whose formation, instead of remaining the clear potential-determining step, has roughly the same equilibrium potential as *CHOO. Theoretical limiting potentials are within reasonable limits of experimental onset.

5.6 Conclusion and outlook

This thesis work give some insight in glycerol electrooxidation mechanisms, but have barely scratched the surface, even if we would restrict ourselves only to thermodynamics. The existing discrepancy between theory and experiment regarding if the first or second group is oxidised first should be further investigated. Different facets can be of interest for such a study, since it has been shown that the mechanism is different on Pt(100) and Pt(111).[159] Kinetics is also a way forward when there are well-established methods to calculate barriers. Cooperation with experimental colleagues with access to good synthesis and analysis, especially in situ, allows for further understanding of the mechanism.

Assuming that the first two step give some information about the full reaction, an easy extension to think of is the addition of alloy or doped surfaces for partial glycerol dehydrogenation. Otherwise, an exhaustive search for deprotonation intermediates on some metals could be useful, as long as surface coverages of *O or *OH are considered at relevant limiting potentials. On platinum, I started calculate every dehydrogenated intermediate, which was time consuming. I would say that the main problem is human time rather that CPU time, so automation of the structure-building process would be a possible continuation. One could imagine moving around the binding adsorbates on surface sites, maintaining bond lengths and tetrahedral angles, and using force fields for a crude pre-relaxation.

Evidence-based addition of explicit and/or implicit solvent effects should be included to get correct adsorption energies. Furthermore, the main reason that we use optB86b-vdW among other exchange-correlation functionals is its accuracy for methanol adsorption on gold, but for screening over other metals, new tests should be carried out.

There is a limit in how far one gets with only thermodynamics. VASPsol in combination with grand-canonical DFT seems promising in my view for calculating barriers, but glycerol is not a good system for trying out electrochemical kinetic models, due to its size. When the research field is more established, electrochemical barriers should be calculated. Something particular from my work that would be interesting to do would be to model the adsorption of protolysed glycerol on the electrode, which is the proposed mechanism in alkaline media, as seen above, to compare with adsorption of (neutral) glycerol.

Computational optimisation of the glycerol electrooxidation reactions is still far away, and the value of solving this problem will only increase along with global usage of biodiesel. Let me finish by quoting Winston Churchill: “Now this is not the end. This is not even the beginning of the end. But it is, perhaps, the end of the beginning.”

Appendix

A Normal mode analysis

In order to find the normal modes of vibration, we need to solve the classical Lagrangian equations. Given a potential energy landscape, in our case calculated with DFT, the forces are computed using a central differential quotient. For further details on this derivation, see Goldstein et al.[143] and Van den Bossche.[160]

Let us expand the potential energy in the vicinity of a stable equilibrium. If x_i denote deviations for atom i, we may expand it in a Maclaurin series:

$$V(x_1, \ldots, x_n) = V(0, \ldots, 0) + \sum_i \Big(\frac{\partial V}{\partial x_i}\Big) x_i + \frac{1}{2} \sum_{i,j} \Big(\frac{\partial^2 V}{\partial x_i \partial x_j}\Big) x_i x_j + \cdots . \tag{5.1}$$

We may choose the potential in the equilibrium to be 0, and, since we have an equilibrium, all forces are zero. Assuming the deviations to be small, we are left with the quadratic terms of the expansion:

$$V = \frac{1}{2} \sum_{i,j} \Big(\frac{\partial^2 V}{\partial x_i \partial x_j}\Big) x_i x_j = \frac{1}{2} \sum_{i,j} V_{ij} x_i x_j \tag{5.2}$$

where V_{ij} is a shorthand notation for the second derivatives of the potential. These can be obtained by sampling the potential energy or the forces around the equilibrium and applying finite differences, or by more elaborate analytic methods mentioned in section 3.4.1.

On matrix form, Equation 5.2 can be written as

$$V = \frac{1}{2} \mathbf{x}^{\mathrm{T}} \mathbf{V} \mathbf{x} \tag{5.3}$$

where $\mathbf{V}$ is the Hessian matrix. By introducing mass-weighted coordinates,[1]

$$q_i = \sqrt{m_i} x_i, \tag{5.4}$$

we can rewrite the Hessian expression to

$$\frac{1}{2} \mathbf{q}^{\mathrm{T}} \mathbf{U} \mathbf{q} \tag{5.5}$$

where $U_{ij} = V_{ij}/(m_i m_j)^{1/2}$. The kinetic energy is given by

$$T = \frac{1}{2} \sum_i m_i \dot{x}_i^2 = \frac{1}{2} \dot{\mathbf{q}}^{\mathrm{T}} \dot{\mathbf{q}} \tag{5.6}$$

[1] Introducing mass-weighted coordinates is just a mathematical trick to simply the expression for kinetic energy. It is possible to do it in a way that is more physically intuitive, at the expense of brevity.

and thus the Lagrangian by

$$L = \frac{1}{2}(\mathbf{q}^{\mathrm{T}}\mathbf{U}\mathbf{q} - \dot{\mathbf{q}}^{\mathrm{T}}\dot{\mathbf{q}}) \tag{5.7}$$

The Lagrangian equations of motion then become

$$\ddot{\mathbf{q}} + \mathbf{U}\mathbf{q} = \mathbf{0}. \tag{5.8}$$

Making the oscillatory ansatz

$$q_j = a_j e^{-i\omega t} \tag{5.9}$$

where a_j are amplitudes and ω the angular frequency, we get

$$(\mathbf{U} - \omega^2\mathbf{I})\mathbf{a} = \mathbf{0} \tag{5.10}$$

which is an eigenvalue problem with matrix $\mathbf{U}$ and eigenvalues ω^2. $\mathbf{U}$ may be written in terms of eigenvectors $\mathbf{P}$ and eigenvalues $\mathbf{\Omega}$ as

$$\mathbf{U} = \mathbf{P}^{\mathrm{T}}\mathbf{\Omega}\mathbf{P}. \tag{5.11}$$

Note that since $\mathbf{U}$ is real and symmetric, $\mathbf{P}$ is orthogonal and thus $\mathbf{P}^{\mathrm{T}} = \mathbf{P}^{-1}$. The potential may be rewritten as

$$\begin{aligned} V &= \frac{1}{2}\mathbf{q}^{\mathrm{T}}(\mathbf{P}^{\mathrm{T}}\mathbf{\Omega}\mathbf{P})\mathbf{q} \\ &= \frac{1}{2}(\mathbf{P}\mathbf{q})^{\mathrm{T}}\mathbf{\Omega}(\mathbf{P}\mathbf{q}) \\ &= \frac{1}{2}\boldsymbol{\zeta}^{\mathrm{T}}\mathbf{\Omega}\boldsymbol{\zeta} \\ &= \frac{1}{2}\sum_i \omega_i^2\xi_i^2. \end{aligned} \tag{5.12}$$

where ζ_i are normal, mass-weighted coordinates. The kinetic energy can be rewritten in these coordinates to

$$\begin{aligned} T &= \frac{1}{2}\dot{\mathbf{q}}^{\mathrm{T}}\dot{\mathbf{q}} \\ &= \frac{1}{2}(\mathbf{P}^{\mathrm{T}}\dot{\boldsymbol{\zeta}})^{\mathrm{T}}(\mathbf{P}^{\mathrm{T}}\dot{\boldsymbol{\zeta}}) \\ &= \frac{1}{2}\dot{\boldsymbol{\zeta}}^{\mathrm{T}}\mathbf{P}\mathbf{P}^{\mathrm{T}}\dot{\boldsymbol{\zeta}} \\ &= \frac{1}{2}\dot{\boldsymbol{\zeta}}^{\mathrm{T}}\dot{\boldsymbol{\zeta}}. \end{aligned} \tag{5.13}$$

If the ζ_i are expressed as a linear combination of q_j (which is the practical case in ASE) can be converted to mass-independent coordinates y_i by dividing element-wise with $\sqrt{m_j}$. These would then correspond to actual normal displacements around the equilibrium.

B Partition functions

We can calculate the total gas phase partition function as

$$Z = \frac{z^N}{N!} \tag{5.14}$$

where z is the partition function for a single particle and n is the number of adsorbates. The reason for the simple product is the assumption that the particles do not interact with each other, and the $n!$ factor stems from the fact that gas phase species are indistinguishable.

Since adsorbates are considered fixed on the surface, theu are distinguishable (by their position on the infinite surface). The adsorbate partition function is thus given as

$$Z = z^N. \tag{5.15}$$

The single particle partition function can be written as a Boltzmann sum over all possible energies

$$z = \sum_i e^{-\beta\varepsilon_i}. \tag{5.16}$$

where $\beta = 1/k_{\mathrm{B}}T$. We consider a given total energy level to be separable into independent modes, m, with energy levels j_m, i.e.

$$\varepsilon_i = \varepsilon_{j_1,j_2,\ldots} = \sum_m \varepsilon_{j_m}, \tag{5.17}$$

where each mode m can occupy a separate set of energy levels. This means that we can write z as a product, since

$$z = \sum_i e^{-\beta\varepsilon_i} \tag{5.18}$$

$$= \sum_{j_1,j_2,\ldots} e^{-\beta\sum_m \varepsilon_{j_m}} \tag{5.19}$$

$$= \prod_m \Big(\sum_{j_m} e^{-\beta\varepsilon_{j_m}}\Big) \tag{5.20}$$

$$= \prod_m z_m. \tag{5.21}$$

We consider translational, rotational, and vibrational contributions to the partition function.

B.1 Translation

The simplest model of the system of a monoatomic gas phase is the three-dimensional particle in a box in a quantum mechanical fashion. The energies of a particle in a one-dimensional box of length x is

$$\varepsilon_i = \frac{i^2h^2}{8mx^2} \tag{5.22}$$

The system is large enough to assume that the energy spacing close, i.e. the classical limit. This allows the Boltzmann sum to be replaced by integration according to

$$z_{\mathrm{tr}} = \int_0^\infty \exp\Big(- \frac{u^2 h^2}{8mx^2 k_b T}\Big) du \tag{5.23}$$

With a change of variables, it becomes

$$\begin{aligned} z_{\mathrm{tr}} &= \frac{2x\sqrt{2mk_bT}}{h} \int_0^\infty e^{-v^2} dv \\ &= \frac{\sqrt{\pi}}{2} \frac{2x\sqrt{2mk_BT}}{h} \\ &= \Big(\frac{2\pi m k_B T}{h^2}\Big)^{0.5} x. \end{aligned} \tag{5.24}$$

For a three-dimensional box of volume V, we have

$$z_{\mathrm{tr}} = \Big(\frac{2\pi m k_B T}{h^2}\Big)^{1.5} V. \tag{5.25}$$

Note that the N dependence of the logarithm of the ideal gas partition function is taken care of neatly, since

$$\ln Z = \ln \frac{z^N}{N!} \tag{5.26}$$

$$= N(\ln z_{\mathrm{tr}} + \ln z_{\mathrm{rot}} z_{\mathrm{vib}}) - \ln N! \tag{5.27}$$

$$\approx N\bigg(\ln V + \ln \Big(\frac{2\pi m k_B T}{h^2}\Big)^{1.5} + \ln z_{\mathrm{rot}} z_{\mathrm{vib}} \bigg) - N \ln N - N \tag{5.28}$$

$$= N\bigg(\ln \frac{k_{\mathrm{B}} T}{p} - 1 + \ln \Big(\frac{2\pi m k_B T}{h^2}\Big)^{1.5} + \ln z_{\mathrm{rot}} z_{\mathrm{vib}} \bigg) \tag{5.29}$$

which divided by N (i.e. per particle) is not dependent on the number of particles.

B.2 Rotation

A linear molecule can be modelled as a quantum mechanical rigid rotor,[9] which gives the eigenenergies

$$\varepsilon_i = \frac{i(i+1)h^2}{8\pi^2 I} \tag{5.30}$$

where

$$I = \sum_k m_k r^2 \tag{5.31}$$

is the moment of inertia around the centre of mass.

E.g., for a diatomic molecule we have

$$I = \frac{m_1 m_2}{m_1 + m_2} d^2. \tag{5.32}$$

Taking the $2i+1$ levels of degeneracy into account, the partition function can be written as

$$\frac{1}{\sigma}\sum_i (2i+1)\exp\Big(-\frac{i(i+1)h^2}{8\pi^2 I k_B T}\Big) \tag{5.33}$$

where σ is the symmetry number. A low-symmetry molecules CO, with no rotational degeneracy, has $\sigma = 1$ while symmetric linear molecules like H_2 and CO_2 have $\sigma = 2$.

If the levels are close, which is true for all but the lightest molecules at all but low temperatures (for H_2, the critical temperature is 85 K), the sum can be approximated with the integral

$$\frac{1}{\sigma}\int_0^\infty (2u+1)\exp\Big(-\frac{u(u+1)h^2}{8\pi^2 I k_B T}\Big)du. \tag{5.34}$$

With the substitution $s = 8\pi^2 I k_B T/h^2$ we have

$$\begin{aligned} z_{\text{rot}} &= \frac{1}{\sigma}\int_0^\infty (2u+1)\exp\Big(-\frac{u(u+1)}{s}\Big)du \\ &= \frac{1}{\sigma}e^{1/(4s)}\int_0^\infty 2(u+\frac{1}{2})\exp\Big(-\frac{(u+1/2)^2}{s}\Big)du \\ &= \frac{1}{\sigma}e^{1/(4s)}\int_{1/2}^\infty 2v\exp\Big(-\frac{v^2}{s}\Big)dv \\ &= \frac{1}{\sigma}e^{1/(4s)}\Big[-s\exp\Big(-\frac{v^2}{s}\Big)\Big]_{1/2}^\infty \\ &= \frac{s}{\sigma} \end{aligned} \tag{5.35}$$

$$\tag{5.36}$$

where $v = u + 1/2$. Resubstitution gives

$$z_{\text{rot}} = \frac{8\pi^2 I k_{\text{B}} T}{\sigma h^2} \tag{5.37}$$

In the general case with non-linear polyatomic molecules, the Hamiltonian can be expressed as

$$H = \frac{L_A^2}{2I_A} + \frac{L_B^2}{2I_B} + \frac{L_C^2}{2I_C} \tag{5.38}$$

where L_A, L_B and L_C are angular momenta and I_A, I_B and I_C are eigenvalues of the moments of inertia.[161] However, the quantification of the angular momenta is complex. As an intuitive sketch, consider the integral

$$\int_{-\infty}^\infty\int_{-\infty}^\infty\int_{-\infty}^\infty \exp\Big(-\frac{H(p,q)}{k_{\text{B}}T}\Big) = (2\pi I_A k_{\text{B}}T)^{1/2}(2\pi I_B k_{\text{B}}T)^{1/2}(2\pi I_C k_{\text{B}}T)^{1/2}. \tag{5.39}$$

In order to get the partition function, this integral must be multiplied by a constant. A factor of 2π accounts for a complete rotation while integration over all axes contributes

with 4π. σ corrects overcounting while a factor of h in each dimension takes care of the conversion from momentum p to quantum wavenumber k giving

$$\begin{aligned} z_{\mathrm{rot}} &= \frac{\sqrt{\pi}}{\sigma}\Big(\frac{8\pi I_A k_{\mathrm{B}} T}{h^2}\Big)^{1/2}\Big(\frac{8\pi I_B k_{\mathrm{B}} T}{h^2}\Big)^{1/2}\Big(\frac{8\pi I_C k_{\mathrm{B}} T}{h^2}\Big)^{1/2} \\ &= \frac{\pi^{7/2}}{\sigma h^3}(8k_{\mathrm{B}}T)^{3/2}\sqrt{I_A I_B I_C}. \end{aligned} \tag{5.40}$$

The symmetry number for non-linear molecules is also related to rotational degeneracy; e.g., CH_3OH has $\sigma = 1$, CH_3O^* has $\sigma = 3$ and CH_4 has $\sigma = 12$.

B.3 Vibration

Vibrations can be modelled as j quantum mechanical harmonic oscillators with energies

$$\epsilon_l = \hbar\omega_l(n + 0.5) \tag{5.41}$$

giving

$$z_{\mathrm{vib},l} = \sum e^{-\beta n\hbar\omega_l} = \frac{1}{1 - e^{-\beta\hbar\omega_l}}. \tag{5.42}$$

The zero point energy,

$$\frac{1}{2}\sum_j \hbar\omega_l, \tag{5.43}$$

is added separately to the ground state energy.

$$z_{\mathrm{tr}} = \Big(\frac{2\pi m k_{\mathrm{B}} T}{h^2}\Big)^{1.5} V, \tag{5.44}$$

$$z_{\mathrm{rot}} = \begin{cases} \frac{8\pi^2 I k_{\mathrm{B}} T}{\sigma h^2} & \text{for linear molecules} \\ \frac{\pi^{7/2}}{\sigma h^3}(8k_{\mathrm{B}}T)^{3/2}\sqrt{I_A I_B I_C} & \text{for non-linear molecules} \end{cases} \tag{5.45}$$

and

$$z_{\mathrm{vib},m} = \frac{1}{1 - e^{-\beta\hbar\omega_m}}. \tag{5.46}$$

Acknowledgements

The work presented in this thesis was carried out at the Division of Chemical Physics at the Department of Physics, Chalmers University of Technology, Göteborg, Sweden.

The work was financially supported by the Formas and the Swedish Research Council.

The calculations were performed at NSC (Linköping) and Uppmax (Uppsala) via a SNIC grant.

I would also like to thank:

My main supervisor Anders Hellman, for being an awesome supervisor. Your accessibility and support means a lot to me, and no matter how bad things seems when entering a meeting, I leave it feeling optimistic and encouraged.

My co-supervisor Björn Wickman for all the help inside and outside the laboratory.

My co-supervisor and examiner Henrik Grönbeck for support, fruitful discussions, and realistic time planning.

Egon Campos dos Santos and Lars Pettersson at Stockholm University for all discussions, help and cooperation.

My colleague Adam Arvidsson for being a friendly, supportive, and cooperative colleague with a great sense of humour.

My former colleague Michael Busch for all the help and support, in particular regarding the work with glycerol electrooxidation on gold.

Other former and current colleagues in the Theory Council at Chemical Physics: Unni, Elisabeth, Lin, Yingxin, Lucy, Alvaro, Astrid, Noemi, Matthias, Mikkel, Matej, Baochang, and Chris.

Aadesh, Christian, Alexander, Mattias, Madeleine, and Michael (Bergmann) for good and cheerful cooperation and coexistance in the Electrochemistry lab.

Other former and current colleagues at Chemical Physics, in particular my former office mates Stephan and Pooya, the Electrochemistry group at Gothenburg University, collaborators in the SSF project on alcohol oxidation for energy efficient hydrogen production, and the Competence Centre for Catalysis.

Friends and family, in particular Cecilia, for all your love and support.

Mikael Valter, Göteborg, May 2020

Bibliography

[1] B. Lindström and L. J. Pettersson. A Brief History of Catalysis. *CATTECH* **7**.4 (2003), 130–138. DOI: 10.1023/A:1025001809516.

[2] E. Fulhame. *An Essay on Combustion, with a View to a New Art of Dying and Painting. Wherein the Phlogistic and Antiphlogistic Hypotheses Are Proven Erroneous*. London : Printed for the author, by J. Cooper, 1794.

[3] J. Wisniak. The History of Catalysis. From the Beginning to Nobel Prizes. *Educación química* **21** (2010), 60–69.

[4] J. J. Berzelius. *Årsberättelsen om framsteg i fysik och kemi*. p. 245. Stockholm: Royal Swedish Academy of Sciences, 1835.

[5] Haber, Fritz. *Thermodynamik technischer Gasreaktionen: Sieben Vorlesungen*. R. Oldenburg, 1905.

[6] K. Honkala et al. Ammonia Synthesis from First-Principles Calculations. *Science* **307**.5709 (2005), 555–558. DOI: 10.1126/science.1106435.

[7] A. Hellman et al. "7.17 - Ammonia Synthesis: State of the Bellwether Reaction". *Comprehensive Inorganic Chemistry II (Second Edition)*. Ed. by J. Reedijk and K. Poeppelmeier. Amsterdam: Elsevier, 2013, pp. 459–474. DOI: 10.1016/B978-0-08-097774-4.00725-7.

[8] Y. Ji et al. Strategies to Enhance the Catalytic Performance of ZSM-5 Zeolite in Hydrocarbon Cracking: A Review. *Catalysts* **7**.12 (2017), 367. DOI: 10.3390/catal7120367.

[9] I. Chorkendorff and J. W. Niemantsverdriet. *Concepts of Modern Catalysis and Kinetics*. John Wiley & Sons, 2006.

[10] H. Härelind Ingelsten. *Catalysis for Lean NOx Reduction : Aspects of Catalyst Synthesis and Surface Acidity*. Doktorsavhandlingar vid Chalmers tekniska högskola: Ny serie 2250. Göteborg : Chalmers tekniska högsk., 2005, 2005.

[11] H. Falsig et al. Trends in the Catalytic CO Oxidation Activity of Nanoparticles. *Angewandte Chemie International Edition* **47**.26 (2008). _eprint: https://onlinelibrary.wiley.com 4835–4839. DOI: 10.1002/anie.200801479.

[12] N. M. Martin et al. CO Oxidation and Site Speciation for Alloyed Palladium–Platinum Model Catalysts Studied by in Situ FTIR Spectroscopy. *The Journal of Physical Chemistry C* **121**.47 (2017), 26321–26329. DOI: 10.1021/acs.jpcc.7b07611.

[13] C. H. Hamann, A. Hamnett, and W. Vielstich. *Electrochemistry*. Weinheim : Wiley-VCH, cop. 2007, 2007.

[14] N. I. Kobozev and V. V. Monblanova. Über den Mechanismus der Elektrodiffusion des Wasserstoffes durch Palladium. *Acta Physiochimica U.R.S.S* **1** (1934), 611–650.

[15] B. P. Company. *BP statistical review of world energy*. 67th edition. British Petroleum Company, 2018.

[16] T. R. Anderson, E. Hawkins, and P. D. Jones. CO2, the Greenhouse Effect and Global Warming: From the Pioneering Work of Arrhenius and Callendar to Today's Earth System Models. *Endeavour* **40**.3 (2016), 178–187. DOI: 10.1016/j.endeavour.2016.07.002.

[17] S. Arrhenius and E. S. Holden. On The Influence of Carbonic Acid In The Air Upon The Temperature of the Earth. *Publications of the Astronomical Society of the Pacific* **9**.54 (1897), 14–24.

[18] T. M. L. Wigley and M. E. Schlesinger. Analytical Solution for the Effect of Increasing CO2 on Global Mean Temperature. *Nature* **315**.6021 (1985), 649–652. DOI: 10.1038/315649a0.

[19] G.-R. Walther et al. Ecological Responses to Recent Climate Change. *Nature* **416**.6879 (2002), 389–395. DOI: 10.1038/416389a.

[20] A. Dai. Drought under Global Warming: A Review. *Wiley Interdisciplinary Reviews: Climate Change* **2**.1 (2011), 45–65. DOI: 10.1002/wcc.81.

[21] W. D. Nordhaus. Economic Aspects of Global Warming in a Post-Copenhagen Environment. *Proceedings of the National Academy of Sciences* (2010), 201005985. DOI: 10.1073/pnas.1005985107.

[22] M. M. Rieger, P. D, and D. E. Deem. Skin Moisturizers. II. The Effects of Cosmetic Ingredients on Human Stratum Corneum. *J. Soc. Cosmet. Chem* (1974), 253–262.

[23] M. S. E. Houache, K. Hughes, and E. A. Baranova. Study on Catalyst Selection for Electrochemical Valorization of Glycerol. en. *Sustainable Energy & Fuels* **3**.8 (2019), 1892–1915. DOI: 10.1039/C9SE00108E.

[24] M. Pagliaro et al. From Glycerol to Value-Added Products. en. *Angewandte Chemie International Edition* **46**.24 (2007), 4434–4440. DOI: 10.1002/anie.200604694.

[25] BASF. Tradition of ideas: formic acid. (accessed Mars 12 2020) (). URL: http://%20www.intermediates.basf.com/chemicals/topstory/ideen_tradition.

[26] G. Dodekatos, S. Schünemann, and H. Tüysüz. Recent Advances in Thermo-, Photo-, and Electrocatalytic Glycerol Oxidation. *ACS Catalysis* **8**.7 (2018), 6301–6333. DOI: 10.1021/acscatal.8b01317.

[27] S. Bagheri, N. M. Julkapli, and W. A. Yehye. Catalytic conversion of biodiesel derived raw glycerol to value added products. *Renewable and Sustainable Energy Reviews* **41** (2015), 113–127. DOI: https://doi.org/10.1016/j.rser.2014.08.031. URL: http://www.sciencedirect.com/science/article/pii/S1364032114007072.

[28] C. Hu et al. Catalytic Hydrogenation of CC and CO in Unsaturated Fatty Acid Methyl Esters. *Catalysis Science & Technology* **4**.8 (2014), 2427–2444. DOI: 10.1039/C4CY00267A.

[29] E. Karakaya, C. Nuur, and L. Assbring. Potential Transitions in the Iron and Steel Industry in Sweden: Towards a Hydrogen-Based Future? *Journal of Cleaner Production* **195** (2018), 651–663. DOI: 10.1016/j.jclepro.2018.05.142.

[30] M. Simões, S. Baranton, and C. Coutanceau. Electrochemical Valorisation of Glycerol. en. *ChemSusChem* **5**.11 (2012), 2106–2124. DOI: 10.1002/cssc.201200335.

[31] X. Li and A. Faghri. Review and Advances of Direct Methanol Fuel Cells (DMFCs) Part I: Design, Fabrication, and Testing with High Concentration Methanol Solutions. *Journal of Power Sources* **226** (2013), 223–240. DOI: 10.1016/j.jpowsour.2012.10.061.

[32] S. Arrhenius. Über Die Reaktionsgeschwindigkeit Bei Der Inversion von Rohrzucker Durch Säuren. *Zeitschrift für Physikalische Chemie* **4U**.1 (1889), 226–248. DOI: 10.1515/zpch-1889-0416.

[33] S. R. Logan. The Origin and Status of the Arrhenius Equation. *Journal of Chemical Education* **59**.4 (1982), 279. DOI: 10.1021/ed059p279.

[34] M. Trautz. Das Gesetz der Reaktionsgeschwindigkeit und der Gleichgewichte in Gasen. Bestätigung der Additivität von Cv-3/2R. Neue Bestimmung der Integrationskonstanten und der Moleküldurchmesser. *Zeitschrift für anorganische und allgemeine Chemie* **96**.1 (1916), 1–28. DOI: 10.1002/zaac.19160960102.

[35] *Wikimedia Commons Figure: Catalysis Scheme*. 2018. URL: https://commons.wikimedia.org/wiki/File:CatalysisScheme.png.

[36] P. Sabatier. Hydrogénations et Déshydrogénations Par Catalyse. *Berichte der deutschen chemischen Gesellschaft* **44**.3 (1911), 1984–2001. DOI: 10.1002/cber.19110440303.

[37] M. Argyle et al. Heterogeneous Catalyst Deactivation and Regeneration: A Review. *Catalysts* **5**.1 (2015), 145–269. DOI: 10.3390/catal5010145.

[38] D. V. Schroeder. *An Introduction to Thermal Physics*. International Edition. San Francisco: Addison Wesley Longman, 2000.

[39] W. Nernst. Die elektromotorische Wirksamkeit der Jonen. *Zeitschrift für physikalische Chemie* **4**.1 (1889), 129–181.

[40] P. Spitzer et al. "Reference Electrodes for Aqueous Solutions". *Handbook of Reference Electrodes*. Springer, Berlin, Heidelberg, 2013, pp. 77–143. DOI: 10.1007/978-3-642-36188-3_5.

[41] Y. Cai and A. B. Anderson. The Reversible Hydrogen Electrode: Potential-Dependent Activation Energies over Platinum from Quantum Theory. *The Journal of Physical Chemistry B* **108**.28 (2004), 9829–9833. DOI: 10.1021/jp037126d.

[42] J. Rossmeisl et al. Calculated Phase Diagrams for the Electrochemical Oxidation and Reduction of Water over Pt(111). *The Journal of Physical Chemistry B* **110**.43 (2006), 21833–21839. DOI: 10.1021/jp0631735.

[43] S. A. Akhade et al. A Simple Method to Approximate Electrode Potential-Dependent Activation Energies Using Density Functional Theory. en. *Catalysis Today*. Electrochemical Reduction of Carbon Dioxide by Heterogenous and Homogeneous Catalysts: Experiment and Theory **288** (2017), 63–73. DOI: 10.1016/j.cattod.2017.01.050.

[44] M. Van den Bossche et al. Assessment of Constant-Potential Implicit Solvation Calculations of Electrochemical Energy Barriers for H2 Evolution on Pt. *The Journal of Physical Chemistry C* **123**.7 (2019), 4116–4124. DOI: 10.1021/acs.jpcc.8b10046.

[45] O. Teschke, G. Ceotto b, and E. de Souza. Interfacial Aqueous Solutions Dielectric Constant Measurements Using Atomic Force Microscopy. *Chemical Physics Letters* **326**.3-4 (2000), 328–334. DOI: 10.1016/S0009-2614(00)00780-6.

[46] *Wikimedia Commons Figure: Double Layer*. 2018. URL: https://commons.wikimedia.org/wiki/File:EDLC-Potentialdistribution.png.

[47] B. Wickman. "Nanostructured model electrodes for studies of fuel cell reactions". PhD thesis. 2010.

[48] M. T. M. Koper. Analysis of Electrocatalytic Reaction Schemes: Distinction between Rate-Determining and Potential-Determining Steps. *Journal of Solid State Electrochemistry* **17**.2 (2013), 339–344. DOI: 10.1007/s10008-012-1918-x.

[49] X. Shi et al. Understanding Activity Trends in Electrochemical Water Oxidation to Form Hydrogen Peroxide. *Nature Communications* **8**.1 (2017), 701. DOI: 10.1038/s41467-017-00585-6.

[50] B. Iandolo et al. The Rise of Hematite: Origin and Strategies to Reduce the High Onset Potential for the Oxygen Evolution Reaction. *Journal of Materials Chemistry A* **3**.33 (2015), 16896–16912. DOI: 10.1039/C5TA03362D.

[51] *Performing Cyclic Voltammetry Measurements Using Model 2450-EC or 2460-EC Electrochemistry Lab System*. SJ Electronics. 2016.

[52] J. Perez, E. R. Gonzalez, and H. M. Villullas. Hydrogen Evolution Reaction on Gold Single-Crystal Electrodes in Acid Solutions. *The Journal of Physical Chemistry B* **102**.52 (1998), 10931–10935. DOI: 10.1021/jp9831987.

[53] O. Diaz-Morales et al. Electrochemical Water Splitting by Gold: Evidence for an Oxide Decomposition Mechanism. *Chemical Science* **4**.6 (2013), 2334–2343. DOI: 10.1039/C3SC50301A.

[54] E. Rouya et al. Electrochemical Characterization of the Surface Area of Nanoporous Gold Films. *Journal of The Electrochemical Society* **159**.4 (2012), K97–K102. DOI: 10.1149/2.097204jes.

[55] R. M. L. M. Sandrini et al. Mechanistic Aspects of Glycerol Electrooxidation on Pt(111) Electrode in Alkaline Media. en. *Electrochemistry Communications* **86** (2018), 149–152. DOI: 10.1016/j.elecom.2017.11.027.

[56] M. F. Vitha. *Chromatography: Principles and instrumentation*. Vol. 185. John Wiley & Sons, 2016.

[57] J. K. Nørskov et al. Origin of the Overpotential for Oxygen Reduction at a Fuel-Cell Cathode. *The Journal of Physical Chemistry B* **108**.46 (2004), 17886–17892. DOI: 10.1021/jp047349j.

[58] A. Rendón-Calle, S. Builes, and F. Calle-Vallejo. A Brief Review of the Computational Modeling of CO2 Electroreduction on Cu Electrodes. *Current Opinion in Electrochemistry* (2018). DOI: 10.1016/j.coelec.2018.03.012.

[59] P. Ferrin et al. Reactivity Descriptors for Direct Methanol Fuel Cell Anode Catalysts. *Surface Science* **602**.21 (2008), 3424–3431. DOI: 10.1016/j.susc.2008.08.011.

[60] P. Ferrin and M. Mavrikakis. Structure Sensitivity of Methanol Electrooxidation on Transition Metals. *Journal of the American Chemical Society* **131**.40 (2009), 14381–14389. DOI: 10.1021/ja904010u.

[61] M. Busch et al. Beyond the Top of the Volcano? – A Unified Approach to Electrocatalytic Oxygen Reduction and Oxygen Evolution. *Nano Energy*. Electrocatalysis **29** (2016), 126–135. DOI: 10.1016/j.nanoen.2016.04.011.

[62] R. Frydendal et al. Enhancing Activity for the Oxygen Evolution Reaction: The Beneficial Interaction of Gold with Manganese and Cobalt Oxides. en. *ChemCatChem* **7**.1 (2015), 149–154. DOI: 10.1002/cctc.201402756.

[63] F. Calle-Vallejo and M. T. M. Koper. First-Principles Computational Electrochemistry: Achievements and Challenges. en. *Electrochimica Acta*. ELECTROCHEMICAL SCIENCE AND TECHNOLOGYState of the Art and Future PerspectivesOn the Occasion of the International Year of Chemistry (2011) **84** (2012), 3–11. DOI: 10.1016/j.electacta.2012.04.062.

[64] Q. Zhang and A. Asthagiri. Solvation Effects on DFT Predictions of ORR Activity on Metal Surfaces. en. *Catalysis Today*. Special Issue Honoring Umit S. Ozkan: 2017 ACS Henry H. Storch Award Winner **323** (2019), 35–43. DOI: 10.1016/j.cattod.2018.07.036.

[65] S. M. Bachrach. Microsolvation of Glycine: A DFT Study. *The Journal of Physical Chemistry A* **112**.16 (2008), 3722–3730. DOI: 10.1021/jp711048c.

[66] N. A. Baker. Improving Implicit Solvent Simulations: A Poisson-Centric View. en. *Current Opinion in Structural Biology*. Theory and Simulation/Macromolecular Assemblages **15**.2 (2005), 137–143. DOI: 10.1016/j.sbi.2005.02.001.

[67] K. Mathew, V. S. C. Kolluru, and R. G. Hennig. *VASPsol: Implicit solvation and electrolyte model for density-functional theory*. https://github.com/henniggroup/VASPsol. 2018. DOI: 10.5281/zenodo.2555053. URL: https://github.com/henniggroup/VASPsol.

[68] K. Mathew et al. Implicit solvation model for density-functional study of nanocrystal surfaces and reaction pathways. *J. Chem. Phys.* **140** (2014), 084106. DOI: 10.1063/1.4865107.

[69] A. Bagger et al. "Fundamental Atomic Insight in Electrocatalysis". *Handbook of Materials Modeling: Applications: Current and Emerging Materials*. Springer, 2018, pp. 1–31.

[70] M. H. Hansen and J. Rossmeisl. pH in Grand Canonical Statistics of an Electrochemical Interface. *The Journal of Physical Chemistry C* **120**.51 (2016), 29135–29143. DOI: 10.1021/acs.jpcc.6b09019.

[71] S. Trasatti. The Absolute Electrode Potential: An Explanatory Note (Recommendations 1986). en. *Pure and Applied Chemistry* **58**.7 (1986), 955–966. DOI: 10.1351/pac198658070955.

[72] K. Chan and J. K. Nørskov. Electrochemical Barriers Made Simple. *The Journal of Physical Chemistry Letters* **6**.14 (2015), 2663–2668. DOI: 10.1021/acs.jpclett.5b01043.

[73] E. Skúlason et al. Density Functional Theory Calculations for the Hydrogen Evolution Reaction in an Electrochemical Double Layer on the Pt(111) Electrode. *Physical Chemistry Chemical Physics* **9**.25 (2007), 3241–3250. DOI: 10.1039/B700099E.

[74] E. Skúlason et al. Modeling the Electrochemical Hydrogen Oxidation and Evolution Reactions on the Basis of Density Functional Theory Calculations. *The Journal of Physical Chemistry C* **114**.42 (2010), 18182–18197. DOI: 10.1021/jp1048887.

[75] K. Chan and J. K. Nørskov. Potential Dependence of Electrochemical Barriers from Ab Initio Calculations. *The Journal of Physical Chemistry Letters* **7**.9 (2016), 1686–1690. DOI: 10.1021/acs.jpclett.6b00382.

[76] C. D. Taylor et al. First Principles Reaction Modeling of the Electrochemical Interface: Consideration and Calculation of a Tunable Surface Potential from Atomic and Electronic Structure. *Physical Review B* **73**.16 (2006), 165402. DOI: 10.1103/PhysRevB.73.165402.

[77] J.-S. Filhol and M. Neurock. Elucidation of the Electrochemical Activation of Water over Pd by First Principles. *Angewandte Chemie International Edition* **45**.3

(2006). _eprint: https://onlinelibrary.wiley.com/doi/pdf/10.1002/anie.200502540, 402–406. DOI: 10.1002/anie.200502540.

[78] R. Sundararaman, W. A. Goddard, and T. A. Arias. Grand Canonical Electronic Density-Functional Theory: Algorithms and Applications to Electrochemistry. *The Journal of Chemical Physics* **146**.11 (2017), 114104. DOI: 10.1063/1.4978411.

[79] R. Sundararaman et al. JDFTx: Software for Joint Density-Functional Theory. en. *SoftwareX* **6** (2017), 278–284. DOI: 10.1016/j.softx.2017.10.006.

[80] P. A. M. Dirac. Quantum Mechanics of Many-Electron Systems. *Proc. R. Soc. Lond. A* **123**.792 (1929), 714–733. DOI: 10.1098/rspa.1929.0094.

[81] P. Strange. *Relativistic Quantum Mechanics : With Applications in Condensed Matter and Atomic Physics*. Cambridge : Cambridge Univ. Press, 1998, 1998.

[82] P. A. M. Dirac. The Quantum Theory of the Electron. *Proc. R. Soc. Lond. A* **117**.778 (1928), 610–624. DOI: 10.1098/rspa.1928.0023.

[83] H. Hellmann. *Hans Hellmann: Einführung in Die Quantenchemie: Mit Biografischen Notizen von Hans Hellmann Jr.* Springer-Verlag, 2015.

[84] P. Schwerdtfeger. The Pseudopotential Approximation in Electronic Structure Theory. *ChemPhysChem* **12**.17 (2011), 3143–3155. DOI: 10.1002/cphc.201100387.

[85] R. M. Martin. *Electronic Structure: Basic Theory and Practical Methods*. Cambridge: Cambridge Univ. Press, 2004.

[86] J. Thijssen. *Computational Physics*. Cambridge University Press, 2007.

[87] W. Pauli. Über den Zusammenhang des Abschlusses der Elektronengruppen im Atom mit der Komplexstruktur der Spektren. *Zeitschrift für Physik* **31**.1 (1925), 765–783. DOI: 10.1007/BF02980631.

[88] M. Born and R. Oppenheimer. Zur Quantentheorie Der Molekeln. *Annalen der Physik* **389**.20 (1927), 457–484. DOI: 10.1002/andp.19273892002.

[89] B. I. Lundqvist, A. Hellman, and I. Zorić. Electron Transfer and Nonadiabaticity. *Handbook of Surface Science* **3** (2008), 429–524.

[90] J. Kohanoff. *Electronic Structure Calculations for Solids and Molecules: Theory and Computational Methods*. Cambridge: Cambridge Univ. Press, 2006.

[91] C. Venkataraman, A. V. Soudackov, and S. Hammes-Schiffer. Theoretical Formulation of Nonadiabatic Electrochemical Proton-Coupled Electron Transfer at Metal-Solution Interfaces. *The Journal of Physical Chemistry C* **112**.32 (2008), 12386–12397. DOI: 10.1021/jp802171y.

[92] M. M. Melander et al. Grand-Canonical Approach to Density Functional Theory of Electrocatalytic Systems: Thermodynamics of Solid-Liquid Interfaces at Constant Ion and Electrode Potentials. *The Journal of Chemical Physics* **150**.4 (2018), 041706. DOI: 10.1063/1.5047829.

[93] D. R. Hartree. The Wave Mechanics of an Atom with a Non-Coulomb Central Field. Part I. Theory and Methods. *Mathematical Proceedings of the Cambridge Philosophical Society* **24**.1 (1928), 89–110. DOI: 10.1017/S0305004100011919.

[94] V. Fock. Näherungsmethode zur Lösung des quantenmechanischen Mehrkörperproblems. *Zeitschrift für Physik* **61**.1 (1930), 126–148. DOI: 10.1007/BF01340294.

[95] L. H. Thomas. The Calculation of Atomic Fields. *Mathematical Proceedings of the Cambridge Philosophical Society* **23**.5 (1927), 542–548. DOI: 10.1017/S0305004100011683.

[96] E. Fermi. Un metodo statistico per la determinazione di alcune priorieta dell'atome. *Rend. Accad. Naz. Lincei* **6**.602-607 (1927), 32.

[97] P. Hohenberg and W. Kohn. Inhomogeneous Electron Gas. *Physical Review* **136**.3B (1964), B864–B871. DOI: 10.1103/PhysRev.136.B864.

[98] W. Kohn and L. J. Sham. Self-Consistent Equations Including Exchange and Correlation Effects. *Physical Review* **140**.4A (1965), A1133–A1138. DOI: 10.1103/PhysRev.140.A1133.

[99] J. P. Perdew et al. Prescription for the Design and Selection of Density Functional Approximations: More Constraint Satisfaction with Fewer Fits. *The Journal of Chemical Physics* **123**.6 (2005), 062201. DOI: 10.1063/1.1904565.

[100] D. M. Ceperley and B. J. Alder. Ground State of the Electron Gas by a Stochastic Method. *Physical Review Letters* **45**.7 (1980), 566–569. DOI: 10.1103/PhysRevLett.45.566.

[101] D. C. Langreth and M. J. Mehl. Beyond the Local-Density Approximation in Calculations of Ground-State Electronic Properties. *Physical Review B* **28**.4 (1983), 1809–1834. DOI: 10.1103/PhysRevB.28.1809.

[102] A. D. Becke. Density-Functional Exchange-Energy Approximation with Correct Asymptotic Behavior. *Physical Review A* **38**.6 (1988), 3098–3100. DOI: 10.1103/PhysRevA.38.3098.

[103] J. P. Perdew et al. Atoms, Molecules, Solids, and Surfaces: Applications of the Generalized Gradient Approximation for Exchange and Correlation. *Physical Review B* **46**.11 (1992), 6671–6687. DOI: 10.1103/PhysRevB.46.6671.

[104] J. P. Perdew et al. Erratum: Atoms, Molecules, Solids, and Surfaces: Applications of the Generalized Gradient Approximation for Exchange and Correlation. *Physical Review B* **48**.7 (1993), 4978–4978. DOI: 10.1103/PhysRevB.48.4978.2.

[105] J. P. Perdew, K. Burke, and M. Ernzerhof. Generalized Gradient Approximation Made Simple. *Physical Review Letters* **77**.18 (1996), 3865–3868. DOI: 10.1103/PhysRevLett.77.3865.

[106] J. P. Perdew et al. Accurate Density Functional with Correct Formal Properties: A Step Beyond the Generalized Gradient Approximation. *Physical Review Letters* **82**.12 (1999), 2544–2547. DOI: 10.1103/PhysRevLett.82.2544.

[107] A. D. Becke. A New Mixing of Hartree–Fock and Local Density-functional Theories. *The Journal of Chemical Physics* **98**.2 (1993), 1372–1377. DOI: 10.1063/1.464304.

[108] A. J. Garza and G. E. Scuseria. Predicting Band Gaps with Hybrid Density Functionals. *The Journal of Physical Chemistry Letters* **7**.20 (2016), 4165–4170. DOI: 10.1021/acs.jpclett.6b01807.

[109] R. O. Jones and O. Gunnarsson. The Density Functional Formalism, Its Applications and Prospects. *Reviews of Modern Physics* **61**.3 (1989), 689–746. DOI: 10.1103/RevModPhys.61.689.

[110] F. London. The General Theory of Molecular Forces. *Transactions of the Faraday Society* **33**.0 (1937), 8b–26. DOI: 10.1039/TF937330008B.

[111] E. Hult et al. Density Functional for van Der Waals Forces at Surfaces. *Physical Review Letters* **77**.10 (1996), 2029–2032. DOI: 10.1103/PhysRevLett.77.2029.

[112] S. Grimme. Semiempirical GGA-type density functional constructed with a long-range dispersion correction. *Journal of Computational Chemistry* **27**.15 (2006), 1787–1799. DOI: 10.1002/jcc.20495.

[113] J. E. Jones. On the Determination of Molecular Fields. —II. From the Equation of State of a Gas. *Proc. R. Soc. Lond. A* **106**.738 (1924), 463–477. DOI: 10.1098/rspa.1924.0082.

[114] J. F. Dobson. Beyond Pairwise Additivity in London Dispersion Interactions. *International Journal of Quantum Chemistry* **114**.18 (2014), 1157–1161. DOI: 10.1002/qua.24635.

[115] M. Dion et al. Van Der Waals Density Functional for General Geometries. *Physical Review Letters* **92**.24 (2004), 246401. DOI: 10.1103/PhysRevLett.92.246401.

[116] D. C. Langreth et al. Van der Waals density functional theory with applications. *International Journal of Quantum Chemistry* **101**.5 (2005), 599–610. DOI: 10.1002/qua.20315.

[117] Y. Zhang and W. Yang. Comment on "Generalized Gradient Approximation Made Simple". *Physical Review Letters* **80**.4 (1998), 890–890. DOI: 10.1103/PhysRevLett.80.890.

[118] A. D. Becke. Density Functional Calculations of Molecular Bond Energies. *The Journal of Chemical Physics* **84**.8 (1986), 4524–4529. DOI: 10.1063/1.450025.

[119] A. D. Becke. On the Large-gradient Behavior of the Density Functional Exchange Energy. *The Journal of Chemical Physics* **85**.12 (1986), 7184–7187. DOI: 10.1063/1.451353. (Visited on 04/19/2017).

[120] J. Klimeš, D. R. Bowler, and A. Michaelides. Chemical Accuracy for the van Der Waals Density Functional. *Journal of Physics: Condensed Matter* **22**.2 (2010), 022201. DOI: 10.1088/0953-8984/22/2/022201.

[121] J. Klimeš, D. R. Bowler, and A. Michaelides. Van Der Waals Density Functionals Applied to Solids. *Physical Review B* **83**.19 (2011), 195131. DOI: 10.1103/PhysRevB.83.195131.

[122] J. Wellendorff et al. Density Functionals for Surface Science: Exchange-Correlation Model Development with Bayesian Error Estimation. *Physical Review B* **85**.23 (2012), 235149. DOI: 10.1103/PhysRevB.85.235149.

[123] O. Gunnarsson, B. I. Lundqvist, and S. Lundqvist. Screening in a Spin-Polarized Electron Liquid. *Solid State Communications* **11**.1 (1972), 149–153. DOI: 10.1016/0038-1098(72)91150-7.

[124] O. Gunnarsson and B. I. Lundqvist. Exchange and Correlation in Atoms, Molecules, and Solids by the Spin-Density-Functional Formalism. *Physical Review B* **13**.10 (1976), 4274–4298. DOI: 10.1103/PhysRevB.13.4274.

[125] J. P. Perdew and S. Kurth. "Density Functionals for Non-Relativistic Coulomb Systems". *Density Functionals: Theory and Applications*. Lecture Notes in Physics. Springer, Berlin, Heidelberg, 1998, pp. 8–59. DOI: 10.1007/BFb0106732.

[126] B. M. Deb. Note on an Upper Bound Property of Second Derivatives of the Energy. *Chemical Physics Letters* **17**.1 (1972), 78–79. DOI: 10.1016/0009-2614(72)80329-4.

[127] M. E. H. Ismail and M. E. Muldoon. On the Variation with Respect to a Parameter of Zeros of Bessel and Q-Bessel Functions. *Journal of Mathematical Analysis and Applications* **135**.1 (1988), 187–207. DOI: 10.1016/0022-247X(88)90148-5.

[128] H. Jacobsen et al. Analytic Second Derivatives of Molecular Energies: A Density Functional Implementation. *Computer Physics Communications* **100**.3 (1997), 263–276. DOI: 10.1016/S0010-4655(96)00119-1.

[129] H. Nakata et al. Analytic Second Derivative of the Energy for Density Functional Theory Based on the Three-Body Fragment Molecular Orbital Method. *The Journal of Chemical Physics* **142**.12 (2015), 124101. DOI: 10.1063/1.4915068.

[130] R. I. Delgado-Venegas et al. Analytic Second Derivatives from Auxiliary Density Perturbation Theory. *The Journal of Chemical Physics* **145**.22 (2016), 224103. DOI: 10.1063/1.4971292.

[131] G. Kresse and J. Furthmüller. Efficiency of Ab-Initio Total Energy Calculations for Metals and Semiconductors Using a Plane-Wave Basis Set. *Computational Materials Science* **6**.1 (1996), 15–50. DOI: 10.1016/0927-0256(96)00008-0.

[132] G. Kresse and J. Furthmüller. Efficient Iterative Schemes for Ab Initio Total-Energy Calculations Using a Plane-Wave Basis Set. *Physical Review B* **54**.16 (1996), 11169–11186. DOI: 10.1103/PhysRevB.54.11169.

[133] H. J. Monkhorst and J. D. Pack. Special Points for Brillouin-Zone Integrations. *Physical Review B* **13**.12 (1976), 5188–5192. DOI: 10.1103/PhysRevB.13.5188.

[134] M. Michelini, R. Pis Diez, and A. Jubert. A density functional study of small nickel clusters. *International journal of quantum chemistry* **70**.4-5 (1998), 693–701.

[135] M. P. Allen and D. J. Tildesley. *Computer Simulation of Liquids*. Oxford University Press, 1987.

[136] E. Braun, S. M. Moosavi, and B. Smit. Anomalous Effects of Velocity Rescaling Algorithms: The Flying Ice Cube Effect Revisited. *Journal of Chemical Theory and Computation* **14**.10 (2018), 5262–5272. DOI: 10.1021/acs.jctc.8b00446.

[137] S. Nosé. A Unified Formulation of the Constant Temperature Molecular Dynamics Methods. *The Journal of Chemical Physics* **81**.1 (1984), 511–519. DOI: 10.1063/1.447334.

[138] W. G. Hoover. Canonical Dynamics: Equilibrium Phase-Space Distributions. *Physical Review A* **31**.3 (1985), 1695–1697. DOI: 10.1103/PhysRevA.31.1695.

[139] S. Nosé. Constant Temperature Molecular Dynamics Methods. en. *Progress of Theoretical Physics Supplement* **103** (1991), 1–46. DOI: 10.1143/PTPS.103.1.

[140] D. M. Bylander and L. Kleinman. Energy Fluctuations Induced by the Nos\'e Thermostat. *Physical Review B* **46**.21 (1992), 13756–13761. DOI: 10.1103/PhysRevB.46.13756.

[141] A. Vojvodic. "Reactivity of transition-metal compounds from electronic structure". Doctoral Thesis. 2009.

[142] F. Abild-Pedersen et al. Scaling Properties of Adsorption Energies for Hydrogen-Containing Molecules on Transition-Metal Surfaces. *Physical Review Letters* **99**.1 (2007), 016105. DOI: 10.1103/PhysRevLett.99.016105.

[143] C. P. P. J. L. Safko, H. Goldstein, and C. Poole. *Classical mechanics*. Pearson Education, Inc, 2002.

[144] P. Stoltze. Surface Science as the Basis for the Understanding of the Catalytic Synthesis of Ammonia. *Physica Scripta* **36**.5 (1987), 824. DOI: 10.1088/0031-8949/36/5/010.

[145] *Atomic Simulation Environment*. 2018. URL: https://wiki.fysik.dtu.dk/ase/ase/thermochemistry/thermochemistry.html.

[146] M. Jørgensen and H. Grönbeck. Adsorbate Entropies with Complete Potential Energy Sampling in Microkinetic Modeling. *The Journal of Physical Chemistry C* **121**.13 (2017), 7199–7207. DOI: 10.1021/acs.jpcc.6b11487.

[147] H. A. Hansen, J. Rossmeisl, and J. K. Nørskov. Surface Pourbaix Diagrams and Oxygen Reduction Activity of Pt, Ag and Ni(111) Surfaces Studied by DFT. *Physical Chemistry Chemical Physics* **10**.25 (2008), 3722–3730. DOI: 10.1039/B803956A.

[148] E. G. Shay. Diesel Fuel from Vegetable Oils: Status and Opportunities. en. *Biomass and Bioenergy* **4**.4 (1993), 227–242. DOI: 10.1016/0961-9534(93)90080-N.

[149] A. Kahyaoglu, B. Beden, and C. Lamy. Oxydation electrocatalitique du glycerol sur electrodes d'or et de platine en milieu aqueux. *Electrochimica Acta* **29**.10 (1984), 1489–1492. DOI: 10.1016/0013-4686(84)87033-4.

[150] C. Lamy et al. Recent Advances in the Development of Direct Alcohol Fuel Cells (DAFC). en. *Journal of Power Sources*. 7th Ulmer Elektrochemische Tage **105**.2 (2002), 283–296. DOI: 10.1016/S0378-7753(01)00954-5.

[151] D. T. Johnson and K. A. Taconi. The Glycerin Glut: Options for the Value-Added Conversion of Crude Glycerol Resulting from Biodiesel Production. en. *Environmental Progress* **26**.4 (2007), 338–348. DOI: 10.1002/ep.10225.

[152] B. Liu and J. Greeley. Decomposition Pathways of Glycerol via C–H, O–H, and C–C Bond Scission on Pt(111): A Density Functional Theory Study. *The Journal of Physical Chemistry C* **115**.40 (2011), 19702–19709. DOI: 10.1021/jp202923w.

[153] B. Liu and J. Greeley. Density Functional Theory Study of Selectivity Considerations for C–C Versus C–O Bond Scission in Glycerol Decomposition on Pt(111). en. *Topics in Catalysis* **55**.5-6 (2012), 280–289. DOI: 10.1007/s11244-012-9806-2.

[154] B. Liu and J. Greeley. A Density Functional Theory Analysis of Trends in Glycerol Decomposition on Close-Packed Transition Metal Surfaces. en. **15**.17 (2013), 6475–6485. DOI: 10.1039/C3CP44088E.

[155] Y. Chen, M. Salciccioli, and D. G. Vlachos. An Efficient Reaction Pathway Search Method Applied to the Decomposition of Glycerol on Platinum. *The Journal of Physical Chemistry C* **115**.38 (2011), 18707–18720. DOI: 10.1021/jp205483m.

[156] Y. Kwon et al. Electrocatalytic Oxidation of Alcohols on Gold in Alkaline Media: Base or Gold Catalysis? *Journal of the American Chemical Society* **133**.18 (2011), 6914–6917. DOI: 10.1021/ja200976j.

[157] Y. Kwon, K. J. P. Schouten, and M. T. M. Koper. Mechanism of the Catalytic Oxidation of Glycerol on Polycrystalline Gold and Platinum Electrodes. *ChemCatChem* **3**.7 (2011), 1176–1185. DOI: 10.1002/cctc.201100023.

[158] B. Beden et al. Electrocatalytic Oxidation of Saturated Oxygenated Compounds on Gold Electrodes. *Journal of Catalysis* **104**.1 (1987), 37–46. DOI: 10.1016/0021-9517(87)90334-4.

[159] A. C. Garcia et al. Strong Impact of Platinum Surface Structure on Primary and Secondary Alcohol Oxidation during Electro-Oxidation of Glycerol. *ACS Catalysis* **6**.7 (2016), 4491–4500. DOI: 10.1021/acscatal.6b00709.

[160] M. Van den Bossche. "Methane Oxidation over Palladium Oxide: From Electronic Structure to Catalytic Conversion". Licentiate Thesis. 2015.

[161] *Chemistry Libre Texts*. 2018. URL: https://bit.ly/2oqtPMK.